# Metabolic turnover and dynamics of RNA modifications by 13C labelling

**Paulo A Gameiro** ( paulo.gameiro@crick.ac.uk )
University College London

**Iosifina P Foskolou**
Department of Physiology, Development and Neuroscience, University of Cambridge

**Vesela Encheva**
Proteomics Science Technology Platform, Francis Crick Institute

**Mariana Silva dos Santos**
Francis Crick Institute https://orcid.org/0000-0003-2404-8490

**James I MacRae**
The Francis Crick Institute https://orcid.org/0000-0002-1464-8583

**Randall S Johnson**
Department of Cell and Molecular Biology (CMB), Karolinska Institutet

**Jernej Ule**
The Francis Crick Institute https://orcid.org/0000-0002-2452-4277

**Method Article**

**Keywords:** 13C labelling, RNA modifications, mass spectrometry, ribonucleosides, mRNA, tRNA, rRNA, N6-methyladenosine (m6A), N6,N6-dimethyladenosine (m62A), 7-methylguanosine (m7G), metabolic turnover, RNA turnover, methylation dynamics, steady-state, ribonucleotide biosynthesis, T-cell activation, metabolic stress

**Posted Date:** February 26th, 2021

**DOI:** https://doi.org/10.21203/rs.3.rs-109009/v2

**Title: Metabolic turnover and dynamics of RNA modifications by $^{13}C$ labelling**

Authors: Paulo A. Gameiro[1]*, Iosifina P. Foskolou[2,3], Vesela Encheva[5], Mariana Silva Dos Santos[4], James I MacRae[4], Randall S. Johnson[2,3], and Jernej Ule[1]*

* co-corresponding. Electronic address: jernej.ule@crick.ac.uk, paulo.gameiro@crick.ac.uk

[1] RNA Networks Laboratory, Francis Crick Institute, London, UK; Department of Neuromuscular Diseases, UCL Queen Square Institute of Neurology, London, UK. [2]Department of Physiology, Development and Neuroscience, University of Cambridge, Cambridge, UK. [3]Department of Cell and Molecular Biology (CMB), Karolinska Institutet, Stockholm, Sweden. [4]Metabolomics Science Technology Platform, Francis Crick Institute, London, UK. [5]Proteomics Science Technology Platform, Francis Crick Institute, London, UK.

## Abstract

RNA methylation regulates various aspects of RNA metabolism, and dynamic modulation of RNA modifications has emerged as a major effector in cellular transitions. Yet, we lack quantitative methods to comprehensively assess methylation dynamics, its features and regulatory inputs, across RNA modifications. We developed $^{13}C$-dynamods, an isotopic labelling approach using [$^{13}C$-methyl]-methionine, to quantify the turnover of base modifications in newly synthesized RNA. This turnover-based approach resolved the contributions of mRNA vs. ncRNA modifications within polyadenylated RNA and uncovered the distinct kinetics of *N*6-methyladenosine ($m^6A$) and 7-methylguanosine ($m^7G$) in mRNA. Moreover, we obtained converging evidence indicating presence of *N*6,*N*6-dimethyladenosine ($m^6{}_2A$) in non-ribosomal RNA, in particular tRNA and rapidly decaying RNAs. Finally, we showed that mRNA methylation dynamics is coordinated with ribonucleotide biosynthesis during T-cell activation, and revealed post-transcriptional lability of $m^6A$ upon metabolic stress. Thus, $^{13}C$-dynamods enables studies of origin, maintenance and regulation of RNA modifications under steady-state and non-stationary conditions.

## INTRODUCTION

RNA methylation modulates crucial RNA-protein interactions at various stages of RNA metabolism. Particularly, *N*6-methyladenosine ($m^6A$), a prevalent modification in eukaryotic messenger RNA (mRNA), is recognized by $m^6A$-'reader' RNA-binding proteins (RBPs) involved in pre-mRNA splicing, nuclear export, degradation, and translation[1,2]. Recent applications of next-generation sequencing (NGS) have enabled the transcriptomic profiling of individual mRNA modifications[3–5], which have uncovered the importance of dynamic $m^6A$-modified mRNAs in development[6–10]. Notably, dysregulation of $m^6A$ levels has been linked to cancer, ageing and neurodegeneration[11–17], which can occur via metabolic inhibition of $m^6A$ demethylation[11,12]. Moreover, dynamic tRNA modifications are post-transcriptional sensors of cellular stress[18–21]. Comprehensive studies of individual RNA modifications have been mostly advanced by NGS-based profiling, which relies on chemical, enzymatic and/or antibody-based detection of modified ribonucleosides[3–5]. These methods have provided a wealth of information on the sites of modification across the transcriptome, but are hampered by a lack of high specificity reagents for every modification[3–5]. Furthermore, the effects of differential gene expression make it challenging to quantify general changes in methylation levels, and only limited insight is obtained into biological associations between various modifications. Thus, the forces driving the dynamics of RNA methylation remain poorly understood, and **approaches are needed that can simultaneously quantify multiple modifications across biological contexts**.

Tandem mass spectrometry (LC-MS/MS) is a highly accurate tool, which has so far been applied primarily in two approaches to identify and quantify RNA modifications. The first approach employs LC-MS/MS of intact RNA oligonucleotides to detect multiple modifications with positional information in specific RNA sequences. This approach is chromatographically challenging[22] and requires advanced data mining for unambiguous identification of RNA fragments, therefore it has so far been applied to mainly to abundant short RNAs, such as miRNAs and tRNAs[22–24]. The second approach employs LC-MS/MS of ribonucleosides, often combined with stable isotopes, for sensitive quantification of RNA modifications[18,25–30]. This approach can simultaneously quantify the abundance of multiple modifications in specific RNA classes of interest, and is thus suitable to assess their

dynamics across biological systems[18]. Yet, these methods have so far been applied mainly to abundant ribosomal RNA (rRNA) and tRNA species, because MS detection of mRNA modifications was unreliable due to the potential for contaminations from the more heavily modified ncRNAs. Moreover, changes in the abundance of modified ribonucleosides do not directly inform on the underlying forces driving these changes. These can include changes in RNA methylation or demethylation rates, or in transcription or decay of methylated RNAs. Therefore, **methods are needed that are capable of assessing the origin, temporal dynamics and regulation of multiple RNA modifications simultaneously**.

**To study RNA methylation dynamics, new approaches that can trace newly methylated RNA and its decay through time, i.e. methylation turnover, are needed.** Stable isotope labelling of cultured cells is a well-established method to quantify metabolic fluxes[31–33]. Here, we have employed a quantitative method using [$^{13}$C-methyl]-methionine labelling to quantify the turnover of base modifications ($^{13}$C-dynamods). $^{13}$C-dynamods measures the fraction of isotopologues (m+0, m+1, m+2) in modified ribonucleosides, which enables it to monitor SAM-dependent RNA methylation of newly synthesized RNA with specificity. This enabled us to examine polyadenylated RNAs and ncRNA in mammalian cells, which were distinguished by the different turnover frequencies (in $hr^{-1}$) of modified ribonucleosides, which are inherently linked to the different half-lives of mRNA, rRNA and tRNA[34–36]. We examined the kinetics of RNA methylation turnover within and across RNA classes as well as in free ribonucleosides to obtain new insights into the origin and presence of various mRNA modifications. We assess RNA methylation dynamics at metabolic steady-state, during T-cell activation and metabolic stresses linked to the co-substrates of RNA (de)methylation, which reveals the dynamic modulation of mRNA and tRNA modifications. Thus, the **sensitivity and quantitative nature of $^{13}$C-dynamods demonstrates its capacity for in-depth characterization of RNA methylation dynamics in multiple RNA classes of interest**.

## RESULTS

### $^{13}$C labelling of polyadenylated and ribosomal RNA modifications

S-adenosylmethionine (SAM) is the direct substrate of RNA methylation reactions in eukaryotic cells[37]. To trace the incorporation of SAM into RNA, we cultured human 786O cells in methionine-free DMEM medium supplemented with either unlabelled methionine ('Unlab') or [$^{13}$C-methyl]-methionine and analysed the isotopologues (m+0, m+1, m+2) of modified and unmodified ribonucleosides by tandem mass spectrometry (LC-MS/MS) (Fig. 1a,b). The m+0 isotopologue (e.g. 150.1 *m/z* for m$^6$A) represents the mass of the analysed molecule where all atoms are present as the most common isotope, whereas the m+1 isotopologue (e.g. 151.1 *m/z* for m$^6$A) indicates the mass shift due to $^{13}$C incorporation from the $^{13}$C-labelled methionine tracer or from the natural abundance of $^{13}$C, N, H and O stable isotopes. Here, we analysed the isotopologues of *N*6-methyladenosine (m$^6$A), 7-methylguanosine (m$^7$G), 1-methyladenosine (m$^1$A), *N*6,*N*6-dimethyladenosine (m$^6{}_2$A), 2'-O-methyladensone (Am), 5-methylcytosine (m$^5$C) and unmodified ribonucleosides from digested polyadenylated (polyA+) RNA, large RNA (>200nt) and tRNA. We observed increased m+1 and concomitant decreased m+0 ion counts in modified ribonucleosides from polyA+ and large RNA after 4 and 24 hours of [$^{13}$C-methyl]-methionine labelling, while the abundance of adenosine and guanosine isotopologues was unaltered (Fig. 1c,d, Extended Data Fig. 1a, Supplementary file1, 2). Conceptually, the isotopologue fraction of each ribonucleoside is internally controlled for the amount of pre-existing ribonucleosides (m+0 and naturally labelled m+1). Also, we determined that the $^{13}$C enrichment of intracellular methionine and SAM reaches a 98-100% plateau within 30 minutes and remains constant thereafter (Extended Data Fig. 1b). **Thus, the change in the heavy isotopologue fraction relative to the unlabelled condition indicates SAM-dependent RNA methylation of newly synthesized RNA**, whose turnover we have examined within and across RNA classes. In contrast to singly methylated ribonucleosides, the m$^6{}_2$A modification exhibited an enrichment mostly of the m+2 isotopologue upon $^{13}$C labelling (Extended Data Fig. 1a), and so the m+2 fraction was used to assess m$^6{}_2$A dynamics in subsequent analyses.

**Quantification of isotopologue fractions showed a faster kinetics for $m^6A$, $m^7G$ and $m^5C$ in polyA+ RNAs when compared to large RNA and tRNAs (Fig. 1e),** in accordance with the faster lifecycle of mRNA in mammalian cells[35]. In contrast, the kinetics of $m^1A$, $m^6{}_2A$ and Am methylation was similar between polyA+ and large RNA fractions (Fig. 1e), suggesting that a large portion of the signal for these modifications in the polyA+ fraction might derive from contaminating ribosomal RNA (rRNA). Of note, the isotopologues are analysed on all ribonucleosides from the same polyA+ pool (Extended Data Fig. 1c), so the purity of polyA+ enrichment is the same in all cases. This indicates that the relative abundance in mRNAs vs contaminating ncRNA is much higher for $m^6A$, $m^7G$ and $m^5C$ compared to $m^1A$, $m^6{}_2A$ and Am. Interestingly, we detected $m^6{}_2A$ in tRNA from 786O cells, and its kinetics was different when compared to large RNA (Fig. 1e and Extended Data Fig. 1c).

**Turnover frequencies for identification of bona fide mRNA modifications**

To examine methylation turnover, we cultured cells for 24 hours with [$^{13}$C-methyl]-methionine followed by replacement (chase) with naturally labelled methionine and analysed the isotopologues over time. In accordance with the preceding findings (Fig. 1e), we observed an exponential decay of the m+1 isotopologue fraction for $m^6A/m^7G$ but not for $Am/m^1A/m^6{}_2A$ in polyA+ RNA (Fig. 2a). Conversely, the modifications of total/large RNAs exhibited uniformly slow turnover (Fig. 2b), consistent with the high stability of rRNA and tRNA in growing cells[34]. To test the kinetic behaviour underlying methylation turnover, we examined the goodness-of-fit of a linear versus exponential regression of the isotopologue fraction. Analysis of residual errors showed that the linear regression ($m_{(t)} = m_{(0)} + kt$) fits well the turnover of $m^1A/m^6{}_2A/Am$ but not $m^6A/m^7G$ in polyA+ RNA, in which the 'U-shaped' curve supports a non-linear model ($m_{(t)} = m_{(0)}\, e^{(-kt)}$) (Fig. 2c, Extended Data Fig. 2a). Conversely, the linear regression fitted well the turnover of ncRNA modifications (Extended Data Fig. 2b,c). The turnover frequency determined for $Am/m^1A/m^6{}_2A$ in polyA+ was similar to ncRNA modifications ($k = 0.031\ hr^{-1}$ on average), and significantly slower than $m^6A$ ($k = 0.244\ hr^{-1}$) or $m^7G$ ($k = 0.089\ hr^{-1}$) in polyA+ RNA (Fig. 2a,b). Thus, **the turnover of $m^1A/m^6{}_2A/Am$ from polyA+ fractions is incompatible with the exponential turnover of mRNA modifications[34,35], confirming that it most likely originates from ncRNA contamination.**

105 The $m^7G$ modification was similar to less abundant than $m^1A$/Am/$m^6{}_2A$ in polyA+ RNA (Fig.
106 2d), and the sensitivity of MS detection was similar between $m^7G$ and $m^1A$/Am/$m^6{}_2A$, as determined
107 from equimolar injections of pure compounds (Extended Data Fig. 2d). Thus, **the distinct turnover of**
108 **polyA+ modifications was not explained by analytical sensitivity or normalised levels alone**, since
109 the levels of modified ribonucleosides were greater in large RNA compared to polyA+ RNA by a factor
110 of 17/37/97/9 for Am/$m^1A$/$m^6{}_2A$/$m^7G$, respectively, while $m^6A$ level was greater in polyA+ RNA by a
111 factor of 2 (Fig. 2e). From the turnover frequency of ncRNA modifications, we estimated that a 50%
112 contribution of ncRNA signal to the ribonucleoside pool in polyA+ RNA would lower the detected
113 turnover of the bona fide $m^6A$ mRNA modification, with a turnover frequency of 0.242$hr^{-1}$, to that of
114 $m^7G$, with a turnover frequency of ~0.09 $hr^{-1}$ (Extended Data Fig. 2e). That is, reliable turnover-based
115 detection of a hypothetical mRNA modification that is more abundant by a factor of 17-97 in ncRNA
116 relative to mRNA will require a maximal ncRNA contamination of 0.5% (50%/97) to 2.9% (50%/17),
117 but even an optimal performance of available methods to purify polyA+ RNA commonly contains over
118 3% of contaminating ncRNA (Extended Data Fig. 2f)[38,39]. Thus, **the ability to resolve bona fide**
119 **mRNA modifications from methylation turnover is limited by the depletion efficiency of highly**
120 **abundant rRNA modifications.**

121 As the turnover frequency of $m^6A$ was ~8 times faster in polyA+ RNA than ncRNA (Fig 2a,b),
122 we reasoned that the $^{13}C$ labelling of free ribonucleosides derived from RNA degradation would consist
123 mostly of degraded mRNA rather than ncRNA. **To interrogate mRNA modifications further with**
124 **higher sensitivity, we examined methylation dynamics in the pool of free ribonucleosides derived**
125 **from metabolic extracts.** We did not include the isotopologue analysis of $m^5C$ in these time-series
126 experiments due to low abundance of its free ribonucleosides, and due to low MS sensitivity for $m^5C$
127 (Fig. 2d, Extended Data Fig. 2d,g), which compromises the quantification under conditions of partial
128 $^{13}C$ labelling. We found that the Michaelis-Menten kinetics following $^{13}C$ labelling was similar for $m^6A$,
129 $m^7G$ and Am (Fig. 2f-h). Interestingly, the $m^6{}_2A$ modification also exhibited a non-linear, faster
130 Michaelis-Menten kinetics than $m^1A$ or 1-methylguanosine ($m^1G$) (Fig. 2f-h), which are known tRNA
131 modifications and were present in the metabolic extracts at high levels (Extended Data Fig. 2g)[40]. Thus,

while the turnover analysis of the polyA+ fraction couldn't be used to validate lowly abundant modifications due to rRNA contamination (Fig. 2e), the turnover of Am and $m^6{}_2A$ in the free pool suggests that these modifications indeed partly derive from mRNA. This was supported by the normalized levels of Am and $m^6{}_2A$ in the free pool being more similar to those of polyA+ than rRNA (Extended Data Fig. 2h). **These results confirm the presence of Am in mRNA**[41] **and suggest m62A is more common in mRNAs than m1A, which has already been studied in mRNAs**[42,43]**.**

## RNA methylation dynamics during T-cell activation

Upon stimulation with T-cell agonists, T cells undergo significant changes in gene expression, signalling and metabolism within hours to support proliferation[44]. We examined RNA methylation turnover in human primary CD8+ T lymphocytes subjected to 4 and 24 hours of *in vitro* activation. **In agreement with our earlier observations, $m^6A$ and $m^7G$ in polyA+ RNA generally exhibited a faster turnover than ncRNA modifications (Fig. 3a-c).** Interestingly, the turnover of $m^7G$ was accelerated in activated T-cells relative to the respective non-activated state, although the variance was high between T-cells from different human healthy donors (Fig. 3a). The turnover of large and tRNA modifications was uniformly accelerated in activated T-cells (Fig. 3b,c). Yet, the methylation turnover varied between tRNA modifications in both T-cell states (Fig. 3c), suggesting a dynamic modulation of each modification at the post-transcriptional level.

The turnover of $m^6A$ in polyA+ was only slightly faster in activated than non-activated T-cells (Fig. 3a), despite the quiescent state that characterizes resting T-cells[44]. Ribonucleotide triphosphates (rNTPs) are synthesized either via salvage or *de novo* synthesis of purines and pyrimidines, and proliferating cells synthesize rNTPs mostly *de novo*[45]. To examine the contribution of anabolic pathways to newly synthesized RNA during T-cell activation, we traced the activity of rNTPs biosynthesis using [3-$^{13}$C]-based serine, which contributes with two carbons to nascent purines (yielding m+2 purine isotopologues)[46]. Indeed, the contribution of purine biosynthesis was higher in activated CD8+ T-cells across RNA classes (Fig. 3d). **Thus, the high $m^6A$ turnover in polyA+ RNA is decoupled from the activity of *de novo* rNTP production in non-activated T-cells. In contrast, the**

**methylation turnover of ncRNA classes is associated with increased activity of rNTP production in T-cell activation**, likely reflecting an increased transcription and ribosomal biogenesis to support cell growth[47].

### Sensitivity of mRNA and ncRNA modifications to metabolic stress

The maintenance and reversibility of DNA/RNA methylation requires SAM and other substrates derived from the central carbon metabolism[48]. We applied $^{13}$C-dynamods to obtain insights into methylation dynamics upon metabolic stresses linked to RNA (de)methylation. **Deprivation of serine or glutamine inhibited mainly the turnover of large RNA modifications (Fig. 4a),** while the normalised levels of large RNA ribonucleosides were unaltered upon stress (Extended Data Fig. 3). This suggests that reduced methylation turnover most likely results from a reduced transcription of rRNA. Interestingly**, glutamine deprivation increased m$^6$A levels in polyA+ RNA (Fig. 4b) even though it did not significantly affect its turnover after 4hr (Fig. 4a)** or in a chase experiment (Fig. 4c). We confirmed that actinomycin (ActD), a pan inhibitor of eukaryotic transcription, completely inhibited the methylation turnover of m$^6$A and m$^7$G in polyA+ RNA (Fig. 4c), in accordance with the co-transcriptional deposition of m$^6$A in mRNA and of most rRNA modifications[49–52]. In contrast to glutamine deprivation, the ActD treatment decreased m$^6$A levels in polyA+ RNA over time (Fig. 4d), recapitulating initial findings of RNA destabilization by m$^6$A RNA methylation[53]. Conversely, m$^7$G levels in polyA+ RNA were unaltered under glutamine deprivation or ActD (Fig. 4d). These data demonstrate the transcriptional sensitivity of ncRNA modifications and post-transcriptional lability of m$^6$A in mRNA in response to metabolic stress.

## DISCUSSION

Isotopic labelling of cultured cells is a well-established method to quantify metabolic activity, but its application to RNA modifications has been limited. Here, we demonstrate that quantification of methylation turnover with dynamic $^{13}$C labelling informs on the distinct dynamics of polyA+ and ncRNA modifications, and their sensitivity to T-cell activation or metabolic perturbations of mammalian cells. **$^{13}$C-dynamods presents several advances in the application of mass spectrometry**

**(MS) techniques to quantify RNA modifications.** First, in contrast to approaches using sequential or multiplexed labelling of ribonucleosides to distinguish between pre-existing and newly synthesized RNA[54,55], the 'heavy' isotopologue fraction derived from [$^{13}$C-methyl]-methionine is internally controlled for the amount of unlabelled, pre-existing ribonucleosides, and is thus specific to modified ribonucleosides. Second, in contrast to nucleotide labelling approaches in which nucleotide recycling within a cell may lead to ineffective chase with unlabeled nucleotides[56,57], a new SAM molecule is required for each (co-transcriptional) methylation cycle in $^{13}$C-dynamods, adding to the specificity and versatility of experimental designs[57]. Third, in contrast to approaches using multiplexing or spiking from isotopically labelled cultures[26,29,55], the dynamic $^{13}$C labelling over time directly inform on the turnover frequency (in $hr^{-1}$)[31,33], because the direct substrate (SAM) of the targeted reaction (RNA methylation) is close to 100% labelled (Extended Data Fig. 1b). Moreover, SAM needs not be fully labelled for comparisons of dynamic $^{13}$C labelling between modifications at early time points as its enrichment is expected to be equal across SAM-dependent RNA modifications. Finally, combined measurements of methylation turnover and ribonucleoside levels allow $^{13}$C-dynamods to also inform on the lability, and thus possible reversibility, of RNA modifications under non-steady state conditions.

Reliable study of mRNA modifications via MS analyses of ribonucleosides is challenging due to the high abundance of heavily modified ncRNAs that can contaminate the polyA+ fraction. To address this challenge, we exploited the different decay rates; mRNA decay is fast, with a median half-life from 40 min to 9 hours in mammalian cells[34,58,59], while rRNA and tRNA exhibit half-lives of 60-70 hours in growing fibroblasts[34]. Using this approach, we could not reliably determine Am/$m^1A$/$m^6{}_2A$ in polyA+ RNA as being derived from mRNAs. Based on methylation turnover, detection of these modifications in polyA+ fraction could result from ncRNA contaminations of 0.5-2.9%, since Am/$m^1A$/$m^6{}_2A$ levels were found higher in ncRNAs by a factor of 17-37-97, respectively. In contrast, a ~6% of ncRNA contamination would be required to fully account for the slower $m^7G$ turnover detected in polyA+ RNA, since $m^7G$ levels were found only ~9 times higher in ncRNAs. A further evidence for the presence of $m^7G$ in mRNAs is the distinct response to metabolic stresses, where turnover of $m^7G$ changed in large RNA but not polyA+ RNA. As the $m^7G$ turnover reflects that of a

bona fide mRNA modification, its slower kinetics in polyadenylated RNA suggests a temporal delay relative to m6A turnover. In this respect, while $m^6A$ is co-transcriptionally deposited in mRNA[49–51], $m^7G$ is an essential modification at the 5' cap of mRNA that can be placed both in the nucleus and cytoplasm[60,61]. Moreover, $m^7G$ sites have been reported within mRNA, catalysed by the cytosolic METTL1 methyltransferase[62]. Taken together, **the distinct kinetics of $m^7G$ and $m^6A$ in polyadenylated RNA suggest compartmentalization differences affecting their temporal deposition into newly synthesized mRNA.**

Previous reports identified $m^5C$ and Am as mRNA modifications[41,63], and more recently also $m^1A$[42,43]. Here, we could not determine the Am and $m^6{}_2A$ as 'mRNA modifications' based on methylation turnover, we could do so by measuring them in the free ribonucleoside pool. **Our analysis of free ribonucleosides showed a similar Michaelis-Menten kinetics for the turnover of Am, $m^6A$ and $m^7G$, consistent with these modifications being derived from the rapidly decaying mRNAs**. This was supported by the normalized levels of free modified ribonucleosides being more similar to those of polyA+ than of ncRNAs. In contrast, the turnover of free $m^1A$ and $m^1G$ ribonucleosides were significantly slower, indicating that these modifications are predominantly derived from a different ncRNA class, likely tRNAs, where they are present at high levels[40]. This aligns with the recent conclusions that $m^1A$ might be restricted to a handful of mRNAs[5,42]. Finally, despite the low sensitivity of $m^5C$ detection in chase experiments, the quantification of $m^5C$ isotopologues at 24 hours is consistent with it $m^5C$ being derived from mRNA[63].

The $m^6{}_2A$ modification is thought to be present primarily in the 18S rRNA of mammalian transcriptomes[64,65], but has not been described in mammalian tRNA or mRNA. While $m^6{}_2A$ has been detected in bacterial tRNA[66], care must be taken with abundant $m^6{}_2A$-modified rRNA fragments that co-purify with tRNA[67], and are not resolved by standard MS quantifications. Here, we detected slower turnover of $m^6{}_2A$ in mammalian tRNAs relative to large RNA, suggesting it is a bona fide and conserved modification of tRNAs. Nevertheless, an unlikely possibility remains that $m^6{}_2A$ is deposited into the contaminant rRNA fragment in a slower fashion as compared to nascent/mature rRNA. Interestingly, the turnover of free $m^6{}_2A$ ribonucleosides exhibited a faster Michaelis-Menten kinetics than $m^1A$/$m^1G$,

canonical ncRNA modifications, suggesting that $m^6{}_2A$ is also present in rapidly-decaying mRNAs. These multiple pieces of evidences suggesting that $m^6{}_2A$ is present in certain mammalian mRNAs and tRNAs merit further investigation. Of note, single methylation intermediates of $m^6{}_2A$ have been detected *in vitro*[68], but we did not detect m+1 isotopologues for $m^6{}_2A$ above its natural abundance. As SAM was 98-100% $^{13}C$-labelled within 30 minutes, the time resolution of our experiments does not capture sequential methylation of adenosine into $m^6{}_2A$. **These various findings highlight the value examining the turnover of RNA modifications to examine the presence of uncharacterised modifications in RNA subclasses**.

Altered methylation turnover can result from changes in methylation rates at the co-transcriptional or post-transcriptional level. We analysed methylation turnover to inform on the dynamics of RNA modifications during T-cell stimulation. We found that the turnover of $m^7G$ in polyA+ RNA was increased upon stimulation, albeit with high variability among T-cell primary samples. It has been reported that S-adenosyl-homocysteine hydrolase (SAHH), which hydrolyses S-adenosyl-homocysteine (SAH) and thus alleviates its feedback inhibition on RNA methyltransferases, is upregulated in T cell activation and boosts $m^7G$ cap methylation during increased gene expression[69]. Whether the nuclear/cytoplasmic capping of $m^7G$[60,61] or internal $m^7G$[62] is dynamically modulated during T-cell activation needs to be examined in more detail. Moreover, the turnover of $m^6A$ was equally fast during T-cell activation despite the fact that *de novo* purine biosynthesis was minimally active in the naïve-like state, as determined using $^{13}C$-labelled serine. This suggests that **CD8+ T-cells initially rely on the salvage and later on the *de novo* pathways to generate nucleotides required to transcribe polyA+ RNA after their stimulation**.

A non-stationary condition may affect the afferent (i.e. transcription) or efferent (i.e. demethylation or degradation) pathways of turnover, which can alter the $^{13}C$ labelling and/or levels of modified ribonucleosides. We observed inhibited turnover of ncRNA methylation under serine deprivation, which is in line with the expected inhibition of mTOR activity and thereby of rRNA biogenesis[70]. In contrast, **glutamine deprivation increased $m^6A$ levels without** changing the turnover (i.e. sum of transcription & mRNA decay) of $m^6A$-containing mRNA, and instead suggests an altered

i) decay of $m^6A$-enriched vs. $m^6A$-depleted RNAs, or ii) dynamics of the $m^6A$ modification itself, such as by decreased methylation. We did not quantify the conversion of $^{13}C$-methyl-groups into *N*6-hydroxymethyladenosine and *N*6-formyladenosine in the cell lines examined[71]. Thus, related developments or orthogonal approaches are needed to address if post-transcriptional dynamics of $m^6A$ by metabolic stress conditions are due to RNA demethylation or preferential degradation of unmodified RNAs. **As glutamine is the main carbon source of α-ketoglutarate, a co-substrate of RNA demethylases[72,73], it is plausible that its depletion could inhibit RNA demethylation**. This supports the notion that the reversibility of $m^6A$ in mRNA is likely context-dependent[74].

**Our study demonstrates how quantification of methylation turnover and abundance with $^{13}C$-dynamods can be used to examine the various forces driving the dynamics of RNA methylations in the major classes of RNAs.** We gain particularly valuable insights into the RNA origin of modifications in polyadenylated RNA, and their dynamics under non-steady state conditions, such as during T-cell activation or upon metabolic stress. These insights open new directions to be further explored by MS and sequencing-based methods that provide information on particular RNAs.

## ACKNOWLEDGMENTS

This project has received funding from Wellcome Trust (103760/Z/14/Z) and the European Research Council (ERC) under the European Union's Seventh Framework Program (FP7/2007-2013)/ERC grant agreement 617837). P.A.G was supported by a Marie Sklodowska-Curie individual fellowship. The Francis Crick Institute receives its core funding from Cancer Research UK (grant no. FC001002), the UK Medical Research Council (grant no. FC001002) and the Wellcome Trust (grant no. FC001002).

## AUTHOR CONTRIBUTIONS

Conceptualization, P.A.G., and J.U.; Methodology, P.A.G, and V.E.; Investigation, P.A.G., and I.P.F.; Formal Analysis, P.A.G., V.E. and M.S.D.S.; Writing – Original Draft, P.A.G., and J.U.; Writing – Review & Editing, P.A.G, I.P.F., J.I.M., R.S.J., and J.U.; Funding Acquisition, J.U.; Resources, P.A.G., I.P.F., J.I.M. and J.U.; Supervision, P.A.G., and J.U.

**CONFLICTS OF INTEREST:** The authors declare no conflicts of interest.

## METHODS

**Cell culture and metabolic labelling.** 786O cells were obtained from the Crick Cell Services and cultured at 37ºC with 5% $CO_2$ in high glucose DMEM medium (ThermoFisher Scientific, #61965026) supplemented with 10% fetal bovine serum (FBS) (ThermoFisher Scientific, #21875034). CD8+ T lymphocytes were cultured in RPMI-1640 (ThermoFisher Scientific, #21875034) supplemented with 10% heat-inactivated FBS (Thermofisher Scientific #10270106), 1% penicillin/streptomycin (Sigma-Aldrich, #P4333) and 30 U/ml IL-2 (Roche, #11011456001). For $^{13}C$ labelling experiments, 786O cells were grown in high glucose DMEM medium without glutamine, methionine and cystine (ThermoFisher Scientific, #21013024) supplemented with 10% dialyzed FBS (ThermoFisher Scientific, #26400044), 2 mM glutamine, 0.1 mM cystine and 0.2 mM [$^{13}C$-methyl]-methionine (CK Isotopes Limited). For labelling T-cells or 786Os in stress conditions, we used custom RPMI and DMEM media (media preparation lab at the Crick) lacking glucose, glutamine, serine and methionine (and otherwise equivalent formulation as commercial versions) supplemented with 11 mM glucose, 2 mM glutamine, 0.4 mM serine (or [3-$^{13}C$]-serine) and 0.2 mM [$^{13}C$-methyl]-methionine (or methionine). 786O cells were grown until 50-60% confluence before switching to $^{13}C$-labelled medium for the indicated time periods. 786O cells were maintained at 50-60% confluence (or 30-40% in chase experiments) and washed with PBS before switching to $^{13}C$-labelled medium (or regular medium in chase) for the indicated time periods. Total CD8+ T-cells isolated from healthy donor were centrifuged, washed with PBS, and 10-20 million cells were activated in $^{13}C$-labelled or unlabelled medium for the indicated time periods.

**Isolation and activation of CD8+ T-cells.** PBMCs were obtained from healthy donors from Cambridge Bioscience or NHSBT (Addenbrooke's hospital, Cambridge UK), and approved the Human Biology Research Ethics Committee at University of Cambridge (application no: HBREC.2018.11). The PBMC isolation was performed within 8-12 hours after blood collection, and T lymphocytes were isolated with MACS Miltenyi kits (total CD8+ T cells: 130-096-495 or CD8 MicroBeads: 130-045-201 plus FcR blocking:130-059-901) following manufacturer's instructions. Cells were cultured in RPMI-1640 (ThermoFisher Scientific, #21875034) supplemented with 10% heat-inactivated FBS (Thermofisher

Scientific #10270106), 1% penicillin/streptomycin (Sigma-Aldrich, #P4333) and 30 U/ml IL-2 (Roche, #11011456001). Total CD8+ T-cells were activated with aCD3/CD28 beads (1:1 beads-to-cell ratio; Gibco #11132D) for 4 hours and 24 hours after isolation. Cell number and viability were measured by ADAM-MC automated cell counter (NanoEnTek) in RPMI medium.

**RNA purification.** At the conclusion of metabolic labelling, the medium was aspirated and extraction of total RNA was performed with the mirVana isolation kit according to manufacturer's instructions (Thermofisher Scientific, #AM1560). Large (>200nt) RNAs were purified by adding 1/3 volume of 100% ethanol to the aqueous phase recovered from the organic extraction before loading into the filter cartridge of the mirVana Kit. Small (<200nt) RNAs were purified by collecting the total filtrate, addition of 2/3 volume of 100% ethanol and loading into the filter cartridge. Purified small RNAs were subjected to size selection using 15% TBE-Urea gel electrophoresis (Thermofisher Scientific #EC6885BOX), tRNAs sliced and recovered from the gel in 200 mM, 50 mM KOAc, 1 mM EDTA with shaking overnight at 16ºC. Polyadenylated RNA was purified from total/large RNA via two rounds of polyA tail hybridization with Oligo-dT magnetic Dynabeads (ThermoFisher Scientific, #61002).

**LC-MS/MS analysis of ribonucleosides.** Purified RNA (100-250 ng) was digested into ribonucleosides using one unit of nuclease P1 (Sigma-Aldrich, #N8630-1VL) in 25 µl of buffer 25 mM NaCl, 2.5 mM $ZnCl_2$ and 10mM $NaCH_3COO$ pH 5.3 and incubated for 2 hours at 37°C. Subsequently, $NH_4HCO_3$ (100 mM) and 5 units of alkaline phosphatase (CIP) (NEB, #M0525S) were added and the sample incubated for 2 hours (or 20 min, with Quick CIP) at 37°C. Formic acid was added at 0.1% v/v in a final volume of 50 µl and samples were filtered (0.22 µm, Millipore) and 15-20 µl analysed in duplicate by LC-MS. Ribonucleosides were resolved with a C18 reverse phase column (100 x 2.1 mm, 3 µm particle size, Chromex Scientific, #F18-020503) and eluted with a gradient of 0.1% v/v formic acid (solvent A) and 80% acetonitrile in 0.1% formic acid (solvent B) at a flow rate of 0.2 ml/min and 40°C: 100% solvent A for 3 min, 12% solvent B for 12 min, and 100% solvent B for 2 min after which the column was re-equilibrated with 100% solvent A for 3 min (20 min total run time). The ribonucleoside separation was performed using U3000 HPLC (Thermo Scientific) and the detection by a TSQ Quantiva Triple Quadrupole mass spectrometer (TSQ Quantiva, Thermo Scientific) controlled

by the Xcalibur software version 4.0.27 (Thermo Scientific). The HPLC was coupled to the TSQ Quantiva using a HESI (heated electrospray) ion source (Thermo Scientific) operating in positive ionization mode with the following parameters: capillary voltage, 3500V; sheath gas flow, 7.35 l/min; gas temperature, 325C. The first and third quadrupoles (Q1 and Q3) were stringently fixed to 0.2 units of resolution and set to detect the mass of the precursor ribonucleoside ion (Q1) and of the base and ribose product ions (Q3). The ribonucleosides were identified by comparison of the retention time and detected mass transitions to commercially available standards. The collision energies were experimentally defined based on the fragmentation pattern of each ribonucleoside standard and chosen based on the maximum intensity of the base product; the ribose ring was used only as a qualifying transition. The retention time, mass transitions (*m/z*) and collision energies of each ribonucleoside were: adenosine, ~4.1 min, 268.1 -> 136.1 *m/z*, 20 V; guanosine, ~5.4 min, 284.1 -> 135.0 *m/z*, 35.5 V; cytidine, ~1.4 min, 244.2 -> 112.05 *m/z*, 12 V; $m^6A$, ~8.7 min, 282.1 -> 150.1 *m/z*, 20 V; $m^1A$, ~1.8 min, 282.1 -> 150.1 *m/z*, 20V, $m^7G$, ~2.3 min, 298.05 -> 166.1 *m/z*, 20V; $m^5C$, ~1.8 min, 258.2 -> 126.1, *m/z*, 13V; $m^6{}_2A$, ~11.9 min, 296.2 -> 164.1 *m/z*, 22V. Each mass transition above corresponded to the m+0 isotopologue, and increased by one (m+1), two (m+2) and three (m+3) units for detection of the other isotopologues *e.g.* $m^6{}_2A$: 297.2 -> 165.1 (m+1), 298.2 -> 166.1 (m+2), 299.2 -> 167.1 (m+3). The dwell time for each transition was 30 ms for a duty cycle of 930 ms (31 transitions), and 8 to 20 data points per chromatographic peak were obtained for 'short' and 'long' peaks, respectively. A mix of ribonucleoside standards containing 0.5, 1, 5, 10, 50, 100, 500 fmol, 1, 5, 10, 50 or 100 pmol of each ribonucleoside was run in parallel after the biological samples for absolute quantifications, a subset of which is shown in Extended Data Fig. 2d. Data were recorded using the Xcalibur 3.0.63 software (ThermoFisher Scientific) and analysed using Skyline (version 19.1)[75] (Supplementary file1, 2).

**Metabolite extraction and LC-MS analysis of SAM/free ribonucleosides.** At the end of cell culture with [$^{13}$C-methyl]-methionine, metabolic activity quenched by adding ice-cold PBS. Metabolites were extracted by addition of 600 µl ice-cold 1:1 (vol/vol) methanol/water to the cell pellets, samples were transferred to a chilled microcentrifuge tube containing 300µl chloroform and 600µl methanol (1500 µl total, in 3:1:1 vol/vol methanol/water/chloroform). Samples were sonicated in a water bath for 8 min at

4˚C, and centrifuged (13000 rpm) for 10 min at 4˚C. The supernatant containing the extract was transferred to a new tube for evaporation in a speed-vacuum centrifuge, resuspended in 3:3:1 (vol/vol/vol) methanol/water/chloroform (350µl total) to phase separate polar metabolites (upper aqueous phase) from apolar metabolites (lower organic phase), and centrifuged. The aqueous phase was transferred to a new tube for evaporation in a speed-vacuum centrifuge, and resuspended in 100µl water for LC-MS acquisition. LC-MS analysis was performed using a Dionex UltiMate LC system (ThermoFisher Scientific) with a ZIC-pHILIC column (150 mm x 4.6 mm, 5 µm particle, Merck Sequant), as described previously[76]. A 15 min elution gradient of 80% Solvent A (20 mM ammonium carbonate in Optima HPLC grade water, Sigma Aldrich) to 20% Solvent B (acetonitrile Optima HPLC grade, Sigma Aldrich) was used, followed by a 5 min wash of 95:5 Solvent A to Solvent B and 5 min re-equilibration. Other parameters were as follows: flow rate, 300 µL/min; column temperature, 25°C; injection volume, 10 µL; autosampler temperature, 4°C. All metabolites were detected across a mass range of 70-1050 *m/z* using a Q Exactive Orbitrap instrument (ThermoFisher Scientific) with heated electrospray ionization and polarity switching mode at a resolution of 70,000 (at 200 *m/z*). MS parameters were as follows: spray voltage 3.5 kV for positive mode and 3.2 kV for negative mode; probe temperature, 320°C; sheath gas, 30 arbitrary units; auxiliary gas, 5 arbitrary units. Parallel reaction monitoring (PRM) was used at a resolution of 17,500 to confirm the identification of metabolites; collision energies were set individually in HCD (high-energy collisional dissociation) mode. Data were recorded using the Xcalibur 3.0.63 software and analysed using Tracefinder 4.1 (ThermoFisher Scientific) according to the manufacturer's workflows.

**Quantification of methylation turnover.** The isotopologue fractions were defined as the total ion counts of the m+1 isotopologue (except for m+2 in $m^6{}_2A$) relative to the total ion counts of the m+0 plus m+1 isotopologues. The kinetics of isotopologue fractions and goodness-of-fit were determined using the Curve Fitting toolbox of Matlab R2020a (MathWorks) either by a linear regression [f(x) = p1*x + p2] or an exponential fit: a one-term function in the chase experiments [f(x) = a*exp(b*x), Levenberg-Marquardt algorithm] and a two-term function to fit the isotopologue fractions of free ribonucleosides [f(x) = a*exp(b*x) + c*exp(d*x), Levenberg-Marquardt algorithm].

## REFERENCES


1. Gilbert, W. V & Bell, T. A. Messenger RNA modifications: Form, distribution, and function. **352**, (2016).
2. Zhao, B. S., Roundtree, I. A. & He, C. Post-transcriptional gene regulation by mRNA modifications. *Nature Reviews Molecular Cell Biology* (2016). doi:10.1038/nrm.2016.132
3. Capitanchik, C., Toolan-Kerr, P., Luscombe, N. M. & Ule, J. How Do You Identify m6 A Methylation in Transcriptomes at High Resolution? A Comparison of Recent Datasets. *Front. Genet.* **11**, 398 (2020).
4. Helm, M. & Motorin, Y. Detecting RNA modifications in the epitranscriptome: predict and validate. *Nat. Rev. Genet.* **18**, 275–291 (2017).
5. Grozhik, A. V. & Jaffrey, S. R. Distinguishing RNA modifications from noise in epitranscriptome maps. *Nat. Chem. Biol.* **14**, 215–225 (2018).
6. Roundtree, I. A., Evans, M. E., Pan, T. & He, C. Dynamic RNA Modifications in Gene Expression Regulation. *Cell* **169**, 1187–1200 (2017).
7. Frye, M., Harada, B. T., Behm, M. & He, C. RNA modifications modulate gene expression during development. *Science (80-. ).* **361**, 1346–1349 (2018).
8. Batista, P. J. *et al.* m6A RNA Modification Controls Cell Fate Transition in Mammalian Embryonic Stem Cells. *Cell Stem Cell* **15**, 707–719 (2014).
9. Li, H.-B. *et al.* m6A mRNA methylation controls T cell homeostasis by targeting the IL-7/STAT5/SOCS pathways. *Nature* (2017). doi:10.1038/nature23450
10. Yoon, K. J. *et al.* Temporal Control of Mammalian Cortical Neurogenesis by m6A Methylation. *Cell* 877–889 (2017). doi:10.1016/j.cell.2017.09.003
11. Su, R. *et al.* R-2HG Exhibits Anti-tumor Activity by Targeting FTO/m 6 A/MYC/CEBPA Signaling. *Cell* **172**, 90-91.e23 (2017).
12. Qing, Y. *et al.* R-2-hydroxyglutarate attenuates aerobic glycolysis in leukemia by targeting the FTO/m6A/PFKP/LDHB axis. *Mol. Cell* 1–18 (2021). doi:10.1016/j.molcel.2020.12.026
13. Min, K. W. *et al.* Profiling of m6A RNA modifications identified an age-associated regulation of AGO2 mRNA stability. *Aging Cell* **17**, (2018).
14. Wu, Z. *et al.* METTL3 counteracts premature aging via m6A-dependent stabilization of MIS12 mRNA. *Nucleic Acids Res.* **48**, 11083–11096 (2020).
15. Livneh, I., Moshitch-Moshkovitz, S., Amariglio, N., Rechavi, G. & Dominissini, D. The m6A epitranscriptome: transcriptome plasticity in brain development and function. *Nat. Rev. Neurosci.* **21**, 36–51 (2020).
16. Chen, X. *et al.* Down-Regulation of m6A mRNA Methylation Is Involved in Dopaminergic Neuronal Death. *ACS Chem. Neurosci.* **10**, 2355–2363 (2019).
17. Han, M. *et al.* Abnormality of m6A mRNA Methylation Is Involved in Alzheimer's Disease. *Front. Neurosci.* **14**, 1–9 (2020).
18. Chan, C. T. Y. *et al.* A Quantitative Systems Approach Reveals Dynamic Control of tRNA Modifications during Cellular Stress. *PLoS Genet.* **6**, e1001247 (2010).
19. Schaefer, M. *et al.* RNA methylation by Dnmt2 protects transfer RNAs against stress-induced cleavage. *Genes Dev.* **24**, 1590–5 (2010).
20. Blanco, S. *et al.* Aberrant methylation of tRNAs links cellular stress to neuro-developmental disorders. *The EMBO Journal* **33**, 2020–2039 (2014).
21. Gkatza, N. A. *et al. Cytosine-5 RNA methylation links protein synthesis to cell metabolism. PLoS Biology* **17**, (2019).
22. Huber, C. G. & Oberacher, H. Analysis of nucleic acids by on-line liquid chromatography-mass spectrometry. *Mass Spectrom. Rev.* **20**, 310–343 (2001).
23. Kullolli, M., Knouf, E., Arampatzidou, M., Tewari, M. & Pitteri, S. J. Intact MicroRNA analysis using high resolution mass spectrometry. *J. Am. Soc. Mass Spectrom.* **25**, 80–87 (2014).
24. Wein, S. *et al.* A computational platform for high-throughput analysis of RNA sequences and modifications by mass spectrometry. *Nat. Commun.* **11**, 926 (2020).
25. Kellner, S. *et al.* Absolute and relative quantification of RNA modifications via biosynthetic isotopomers. 1–10 (2014). doi:10.1093/nar/gku733

26. Popova, A. M. & Williamson, J. R. Quantitative Analysis of rRNA Modifications Using Stable Isotope Labeling and Mass Spectrometry. (2014).
27. Su, D. *et al.* Quantitative analysis of ribonucleoside modifications in tRNA by HPLC-coupled mass spectrometry. *Nat. Protoc.* **9**, 828–841 (2014).
28. Taoka, M. *et al.* A mass spectrometry-based method for comprehensive quantitative determination of post-transcriptional RNA modifications: The complete chemical structure of Schizosaccharomyces pombe ribosomal RNAs. *Nucleic Acids Res.* **43**, (2015).
29. Waghmare, S. P. & Dickman, M. J. Characterization and quantification of RNA post-transcriptional modifications using stable isotope labeling of RNA in conjunction with mass spectrometry analysis. *Anal. Chem.* **83**, 4894–4901 (2011).
30. Wetzel, C. & Limbach, P. A. Mass spectrometry of modified RNAs: Recent developments. *Analyst* **141**, 16–23 (2016).
31. Jang, C., Chen, L. & Rabinowitz, J. D. Metabolomics and Isotope Tracing. *Cell* **173**, 822–837 (2018).
32. Kelleher, J. K. Flux Estimation Using Isotopic Tracers: Common Ground for Metabolic Physiology and Metabolic Engineering. *Metab. Eng.* **3**, 100–110 (2001).
33. Buescher, J. M. *et al.* A roadmap for interpreting 13C metabolite labeling patterns from cells. *Curr. Opin. Biotechnol.* **34**, 189–201 (2015).
34. Abelson, H. T., Johnson, L. F., Penman, S. & Green, H. Changes in Rna in Relation to Growth of Fibroblast .2. Lifetime of Messenger-Rna, Ribosomal-Rna, and Transfer-Rna in Resting and Growing Cells. *Cell* **1**, 161–165 (1974).
35. Ross, J. mRNA Stability in Mammalian Cells. **59**, 423–450 (1995).
36. Chen-Kiang, S., Nevins, J. R. & Darnell, J. E. N-6-methyl-adenosine in adenovirus type 2 nuclear RNA is conserved in the formation of messenger RNA. *J. Mol. Biol.* **135**, 733–752 (1979).
37. Rana, A. K. & Ankri, S. Reviving the RNA world: An insight into the appearance of RNA methyltransferases. *Front. Genet.* **7**, 1–9 (2016).
38. Zhao, W. *et al.* Comparison of RNA-Seq by poly (A) capture, ribosomal RNA depletion, and DNA microarray for expression profiling. *BMC Genomics* **15**, 1–11 (2014).
39. Cui, P. *et al.* A comparison between ribo-minus RNA-sequencing and polyA-selected RNA-sequencing. *Genomics* **96**, 259–265 (2010).
40. Boccaletto, P. *et al.* MODOMICS: a database of RNA modification pathways. 2017 update. *Nucleic Acids Res.* **46**, D303–D307 (2018).
41. Keith, J. M., Ensinger, M. J. & Moss, B. HeLa cell RNA(2'-O-methyladenosine-N6-)-methyltransferase specific for the capped 5'-end of messenger RNA. *J. Biol. Chem.* **253**, 5033–5039 (1978).
42. Safra, M. *et al.* The m1A landscape on cytosolic and mitochondrial mRNA at single-base resolution. *Nature* **551**, 251–255 (2017).
43. Li, X., Xiong, X., Zhang, M., Wang, K. & Chen, Y. Base-resolution mapping reveals distinct m1A methylome in nuclear- and mitochondrial-encoded transcripts. (2017).
44. Pollizzi, K. N. & Powell, J. D. Integrating canonical and metabolic signalling programmes in the regulation of T cell responses. *Nat. Rev. Immunol.* **14**, 435–446 (2014).
45. Fairbanks, L. D., Bofill, M., Ruckemann, K. & Simmonds, H. A. Importance of ribonucleotide availability to proliferating T-lymphocytes from healthy humans: Disproportionate expansion of pyrimidine pools and contrasting effects of de novo synthesis inhibitors. *J. Biol. Chem.* **270**, 29682–29689 (1995).
46. Labuschagne, C. F., van den Broek, N. J. F., Mackay, G. M., Vousden, K. H. & Maddocks, O. D. K. Serine, but not glycine, supports one-carbon metabolism and proliferation of cancer cells. *Cell Rep.* **7**, 1248–1258 (2014).
47. Hoppe, S. *et al.* AMP-activated protein kinase adapts rRNA synthesis to cellular energy supply. *Proc. Natl. Acad. Sci. U. S. A.* **106**, 17781–17786 (2009).
48. Kinnaird, A., Zhao, S., Wellen, K. E. & Michelakis, E. D. Metabolic control of epigenetics in cancer. *Nat. Rev. Cancer* **16**, 694–707 (2016).
49. Slobodin, B. *et al.* Transcription Impacts the Efficiency of mRNA Translation via Co-transcriptional N6-adenosine. *Cell* **169**, 326-337.e12 (2017).

50. Bertero, A. *et al.* The SMAD2/3 interactome reveals that TGFβ controls m 6 A mRNA methylation in pluripotency. *Nature* **555**, 256–259 (2018).
51. Huang, H. *et al.* Histone H3 trimethylation at lysine 36 guides m6A RNA modification co-transcriptionally. *Nature* **567**, 414–419 (2019).
52. Koš, M. & Tollervey, D. Yeast Pre-rRNA Processing and Modification Occur Cotranscriptionally. *Mol. Cell* **37**, 809–820 (2010).
53. Sommer, S., Lavi, U. & Darnell, J. E. The absolute frequency of labeled N-6-methyladenosine in HeLa cell messenger RNA decreases with label time. *J. Mol. Biol.* **124**, 487–499 (1978).
54. Reichle, V. F. *et al.* Surpassing limits of static RNA modification analysis with dynamic NAIL-MS. *Methods* **156**, 91–101 (2019).
55. Heiss, M., Reichle, V. F. & Kellner, S. Observing the fate of tRNA and its modifications by nucleic acid isotope labeling mass spectrometry: NAIL-MS. *RNA Biol.* **14**, 1260–1268 (2017).
56. Nikolov, E. N. & Dabeva, M. D. Re-utilization of pyrimidine nucleotides during rat liver regeneration. *Biochem. J.* **228**, 27–33 (1985).
57. Wolfe, M. B., Goldstrohm, A. C. & Freddolino, P. L. Global analysis of RNA metabolism using bio-orthogonal labeling coupled with next-generation RNA sequencing. *Methods* **155**, 88–103 (2019).
58. Schwanhäusser, B. *et al.* Global quantification of mammalian gene expression control. *Nature* **473**, 337–42 (2011).
59. Tani, H. *et al.* Genome-wide determination of RNA stability reveals hundreds of short-lived noncoding transcripts in mammals. *Genome Res.* **22**, 1382 (2012).
60. Ramanathan, A., Robb, G. B. & Chan, S. H. mRNA capping: Biological functions and applications. *Nucleic Acids Res.* **44**, 7511–7526 (2016).
61. Galloway, A. & Cowling, V. H. mRNA cap regulation in mammalian cell function and fate. *Biochim. Biophys. Acta - Gene Regul. Mech.* **1862**, 270–279 (2019).
62. Zhang, L. S. *et al.* Transcriptome-wide Mapping of Internal N7-Methylguanosine Methylome in Mammalian mRNA. *Mol. Cell* **74**, 1304-1316.e8 (2019).
63. Squires, J. E. *et al.* Widespread occurrence of 5-methylcytosine in human coding and non-coding RNA. *Nucleic Acids Res.* **40**, 5023–5033 (2012).
64. Taoka, M. *et al.* Landscape of the complete RNA chemical modifications in the human 80S ribosome. *Nucleic Acids Res.* 1–10 (2018). doi:10.1093/NAR/GKY811
65. Kellner, S. *et al.* Profiling of RNA modifications by multiplexed stable isotope labelling. *Chem. Commun.* **50**, 3516–3518 (2014).
66. Chan, C. T. Y. *et al.* Identification of N6,N6-dimethyladenosine in transfer RNA from Mycobacterium bovis bacille calmette-guerin. *Molecules* **16**, 5168–5181 (2011).
67. McCloskey, J. a *et al.* Post-transcriptional modification in archaeal tRNAs: identities and phylogenetic relations of nucleotides from mesophilic and hyperthermophilic Methanococcales. *Nucleic Acids Res.* **29**, 4699–4706 (2001).
68. Ensfelder, T. T. *et al.* ALKBH5-induced demethylation of mono- and dimethylated adenosine. *Chem. Commun. (Camb).* **54**, 8591–8593 (2018).
69. Fernandez-Sanchez, M. E., Gonatopoulos-Pournatzis, T., Preston, G., Lawlor, M. A. & Cowling, V. H. S-Adenosyl Homocysteine Hydrolase Is Required for Myc-Induced mRNA Cap Methylation, Protein Synthesis, and Cell Proliferation. *Mol. Cell. Biol.* **29**, 6182–6191 (2009).
70. Goberdhan, D. C. I., Wilson, C. & Harris, A. L. Amino Acid Sensing by mTORC1: Intracellular Transporters Mark the Spot. *Cell Metab.* **23**, 580–589 (2016).
71. Fu, Y. *et al.* FTO-mediated formation of N6-hydroxymethyladenosine and N6-formyladenosine in mammalian RNA. *Nat. Commun.* **4**, 1798 (2013).
72. Zheng, G. *et al.* ALKBH5 Is a Mammalian RNA Demethylase that Impacts RNA Metabolism and Mouse Fertility. *Mol. Cell* **49**, 18–29 (2013).
73. Gerken, T. *et al.* The obesity-associated FTO gene encodes a 2-oxoglutarate-dependent nucleic acid demethylase. *Science* **318**, 1469–72 (2007).
74. Mauer, J. & Jaffrey, S. R. FTO, m 6 A m , and the hypothesis of reversible epitranscriptomic mRNA modifications. *FEBS Lett.* **592**, 2012–2022 (2018).
75. MacLean, B. *et al.* Skyline: an open source document editor for creating and analyzing

targeted proteomics experiments. *Bioinformatics* **26**, 966–968 (2010).
76. Fets, L. *et al.* MCT2 mediates concentration-dependent inhibition of glutamine metabolism by MOG. *Nat. Chem. Biol.* **14**, 1032–1042 (2018).

FIGURE 1

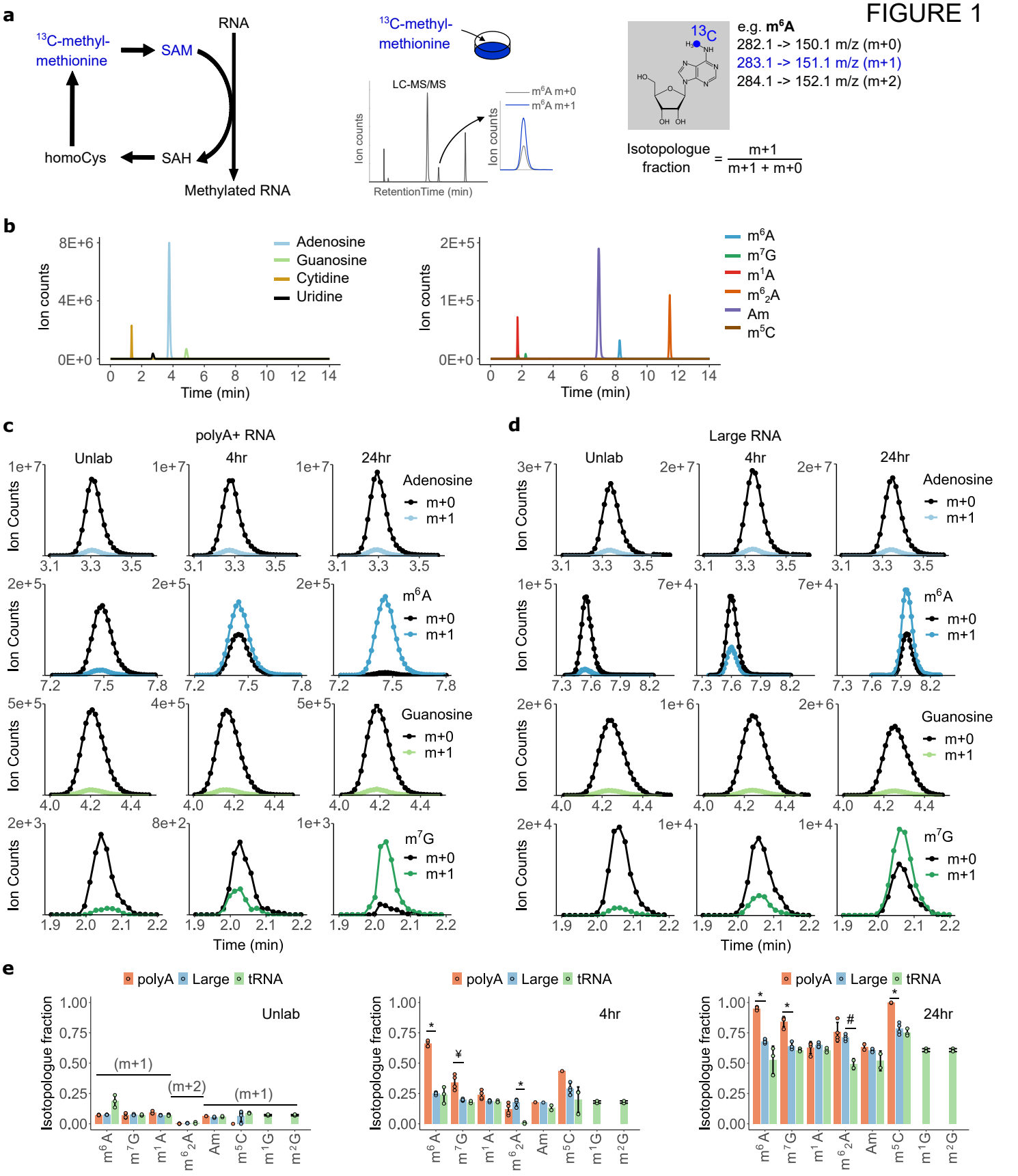


**Figure 1.** **$^{13}$C labelling of RNA modifications across RNA classes. a,** The $^{13}$C-dynamods workflow shows the tracing of RNA methylation: cells are cultured with [$^{13}$C-methyl]-methionine, the RNA is isolated, digested to ribonucleosides and subjected to LC-MS/MS analysis. The isotopologues detected for m$^6$A are shown. **b,** Representative chromatogram of unmodified and modified ribonucleosides from total RNA. **c-d,** The m+0 and m+1 isotopologues of modified and unmodified ribonucleosides (representative chromatograms) in polyA+ (c) and large RNA (d). **e,** Quantification of the isotopologue fractions of each ribonucleoside in polyA+, large and tRNA under unlabelled ('Unlab') conditions, after 4 and 24hours of culture with [$^{13}$C-methyl]-methionine. m$^6$A, *N*6-methyladenosine; m$^7$G, 7-methylguanosine; m$^1$A, 1-methyladenosine; m$^6{}_2$A, *N*6,*N*6-dimethyladenosine; Am, 2′-O-methyladenosine; m$^5$C, 5-methylcytidine; m$^1$G, 1-methylguanosine; m$^2$G, 2-methylguanosine. SAM, s-adenosylmethionine; SAH, s-adenosylhomocysteine; homoCys, homocysteine. Error bars represent standard deviation of three to four biological replicates, with the exception of two replicates for tRNA modifications. In all cases, each replicate is the average of two technical replicas. * denotes P < 0.005, ¥ denotes P < 0.05, # denotes P = 0.059, of a two-sided Student's t-Test comparing samples as indicated.

FIGURE 2

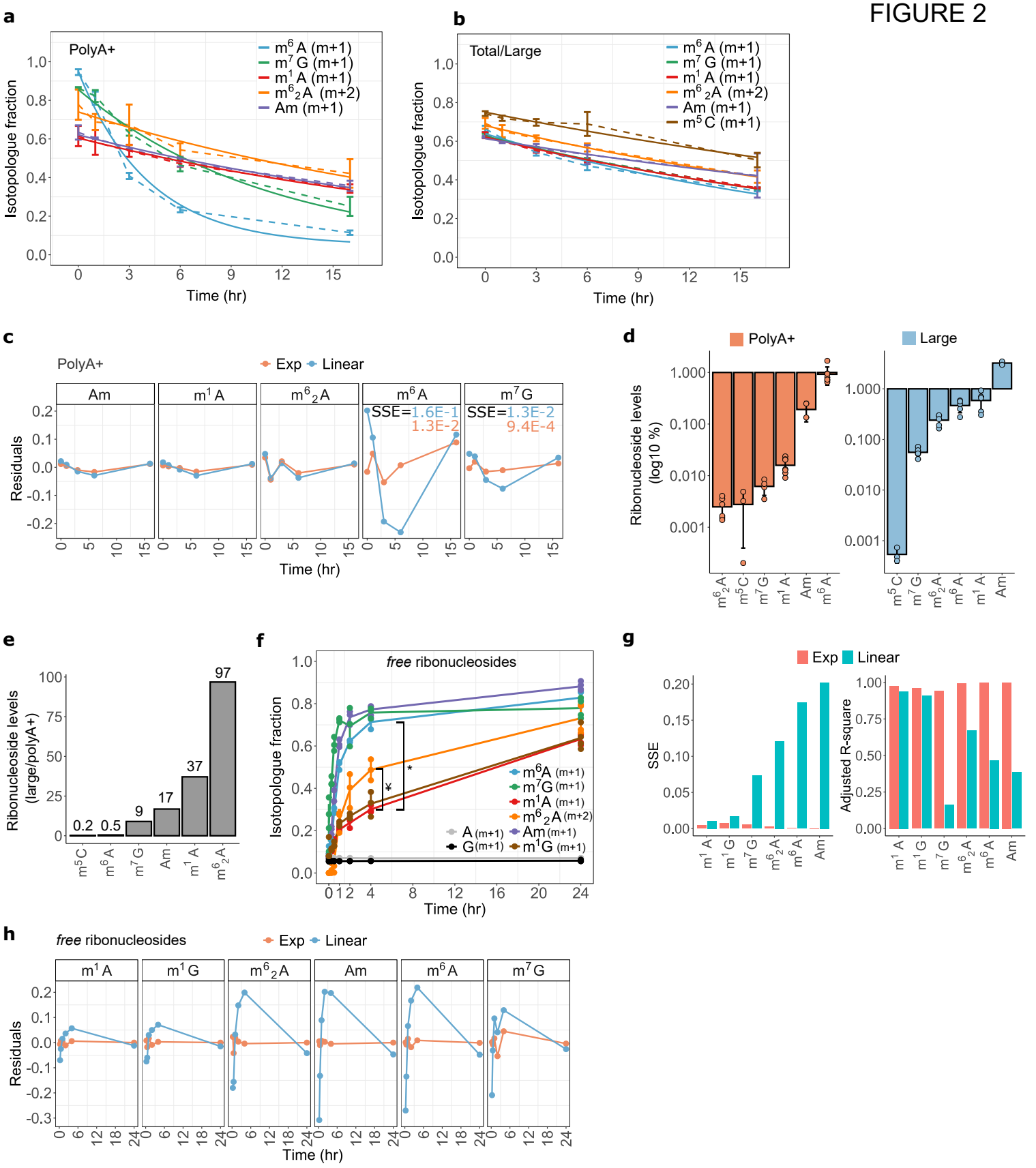


**Figure 2. Kinetic profiling of RNA modifications in polyA+, ncRNA and free ribonucleosides. a-b**, Isotopologue fractions during the 'chase' of $^{13}$C-labelled modifications with naturally labelled methionine for 0, 1, 3, 6 and 16 hours, in polyA+ (a) and total/large RNA (b); dashed lines connect data points; solid lines, exponential (a) or linear (b) fit of isotopologue fractions. **c**, Residuals of a linear vs. exponential regression of isotopologue fractions in polyA+ RNA in the chase experiment. **d,** Normalized ion counts of modified ribonucleosides relative to the ion counts sum of all ribonucleosides, shown for polyA+ and large RNA. (**e**) Ratio of normalised ion counts between polyA+ and large RNA, as determined in (d). **f,** Isotopologue fraction of free ribonucleosides analysed from metabolic extracts. **g-h,** Goodness-of-fit of a linear vs. exponential fit of the isotopologue fractions in free modified ribonucleosides. SSE, sum of squared errors. m$^6$A, *N*6-methyladenosine; m$^7$G, 7-methylguanosine; m$^1$A, 1-methyladenosine; m$^6{}_2$A, *N*6,*N*6-dimethyladenosine; Am, 2′-O-methyladenosine; m$^5$C, 5-methylcytidine; m$^1$G, 1-methylguanosine; A, adenosine; G, guanosine. Error bars represent 90% confidence intervals in (a-b), or standard deviation in (d, f) of at least three biological replicates with exception of Am (two replicates). In all cases, each replicate is the average of two technical replicas. * denotes P < 0.005, ¥ denotes P < 0.05, of a two-sided Student's t-Test comparing m$^6$A and m$^6{}_2$A to m$^1$A, respectively.

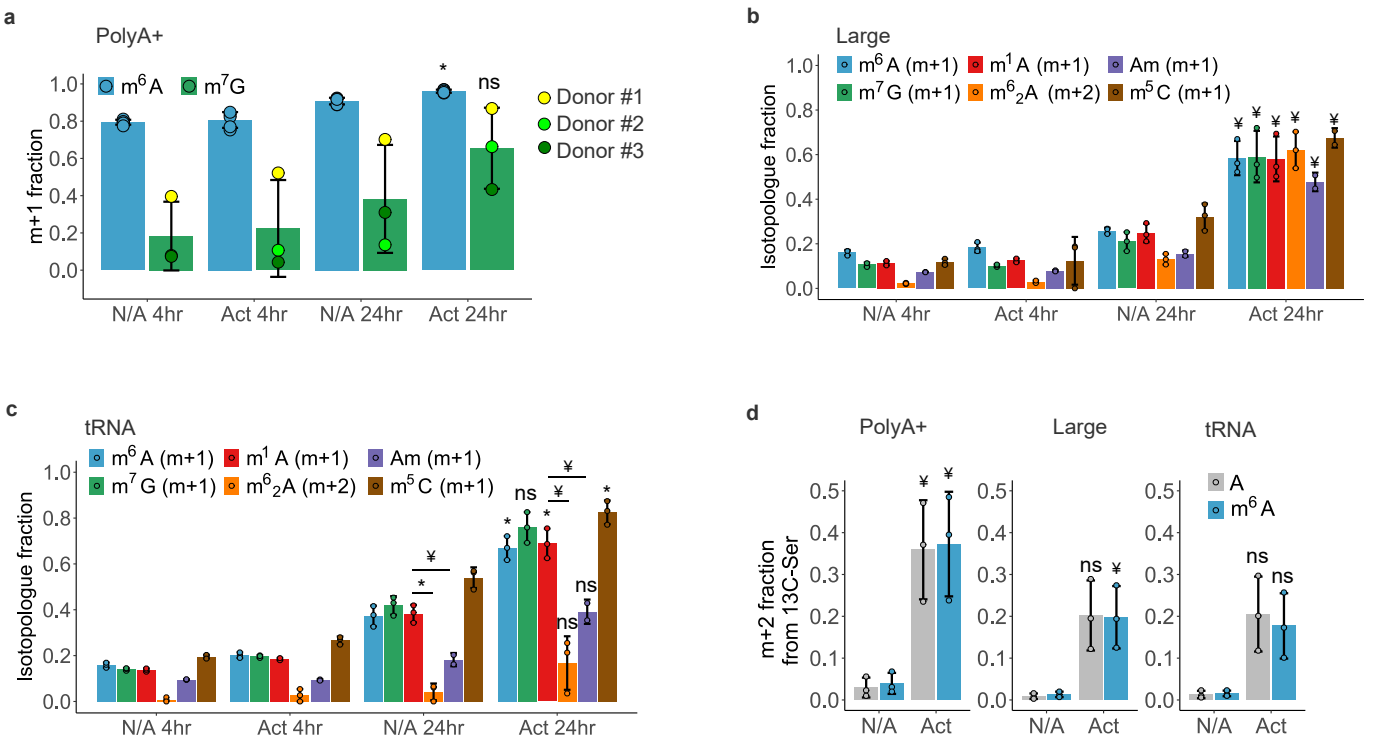


**Figure 3. RNA methylation dynamics during CD8+ T-cell activation. a-c,** Isotopologue fractions of modified ribonucleosides in polyA+ (a), large (b) and tRNA (c) in CD8+ T-cells labelled with $^{13}$C-methyl-methionine for 4 and 24 hours and stimulated with CD3/CD28 antibodies for the same time period. **d,** Quantification of the m+2 fraction from [3-$^{13}$C]serine. N/A, non-activated T-cells; Act, Activated T-cells for the times indicated. Error bars represent standard deviation of T-cell samples from three healthy donors. In all cases, each replicate is the average of two technical replicas. * denotes $P < 0.005$, ¥ denotes $P < 0.05$, ns denotes not significant, of a two-sided Student's t-Test comparing non-activated to activated T-cells at 24 hours or comparing modified ribonucleosides as indicated.

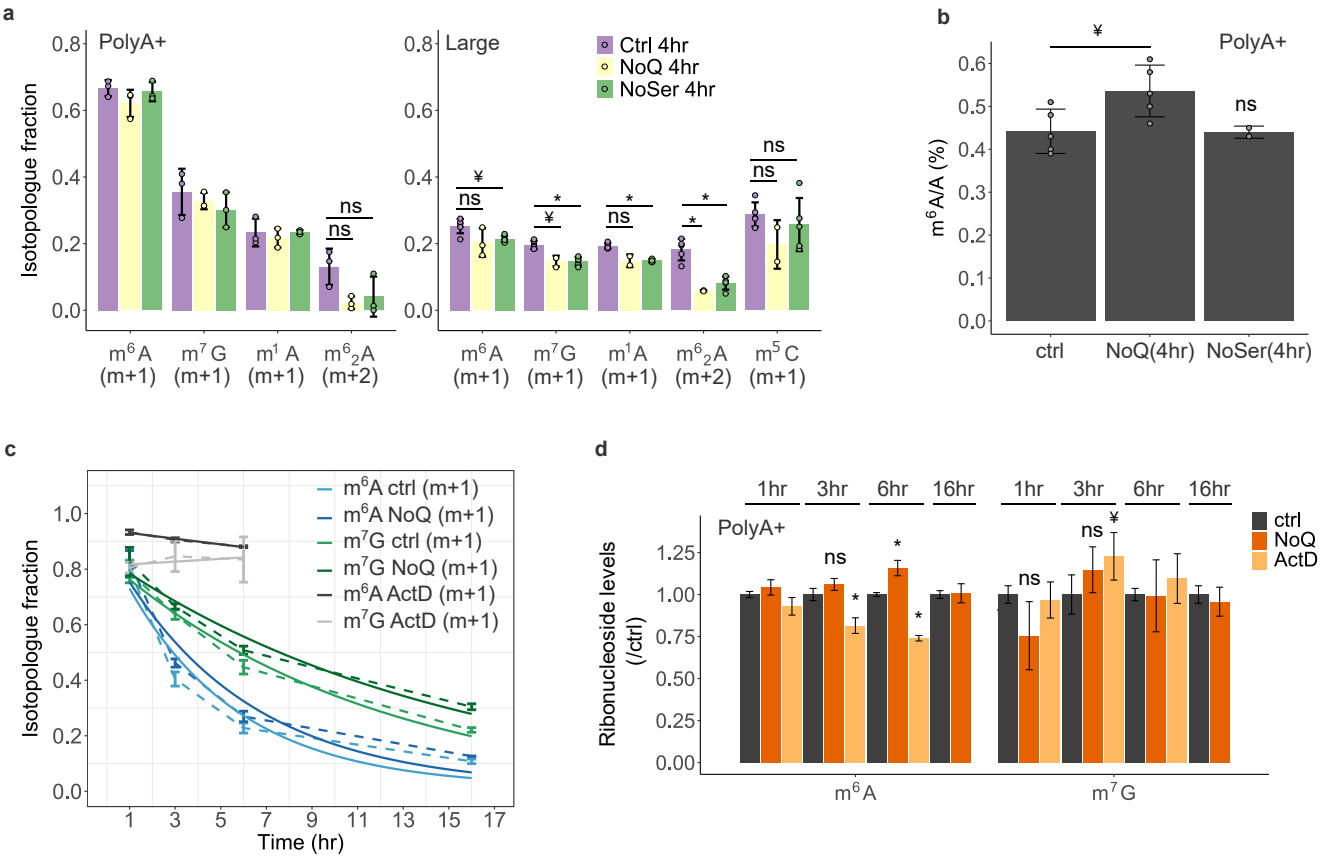


**Figure 4. RNA methylation dynamics under metabolic stress. a,** Isotopologue fractions of modified ribonucleosides in polyA+ and large RNA following [$^{13}$C-methyl]-methionine labelling of 786O cells cultured with complete (ctrl), glutamine- (NoQ), or serine- (NoSer) deprived DMEM medium for 4 hours. **b,** Normalised levels of m$^6$A relative to adenosine in polyA+ RNA from 786O cells cultured with ctrl, NoQ or NoSer DMEM medium for 4 hours. **c**, Isotopologue fractions of m$^6$A and m$^7$G in polyA+ RNA determined from the chase experiment in 786O cells cultured with ctrl, glutamine-deprived (NoQ) DMEM medium or treated with actinomycin D (ActD, 10μM); dashed lines connect data points; solid lines, exponential fit of isotopologue fractions. **d,** Levels of m$^6$A and m$^7$G in polyA+ RNA in the stress conditions as indicated, normalised relative to the ctrl condition in the chase experiment. Error bars represent standard deviation of three or more biological replicates, with exception of (c-d), m$^5$C under NoQ (a) and m$^6$A under NoSer (a) (two biological replicates). In all cases, each replicate is the average of two technical replicas. * denotes $P < 0.005$, ¥ denotes $P < 0.05$, ns denotes not significant, of a two-sided Student's t-Test comparing samples as indicated.

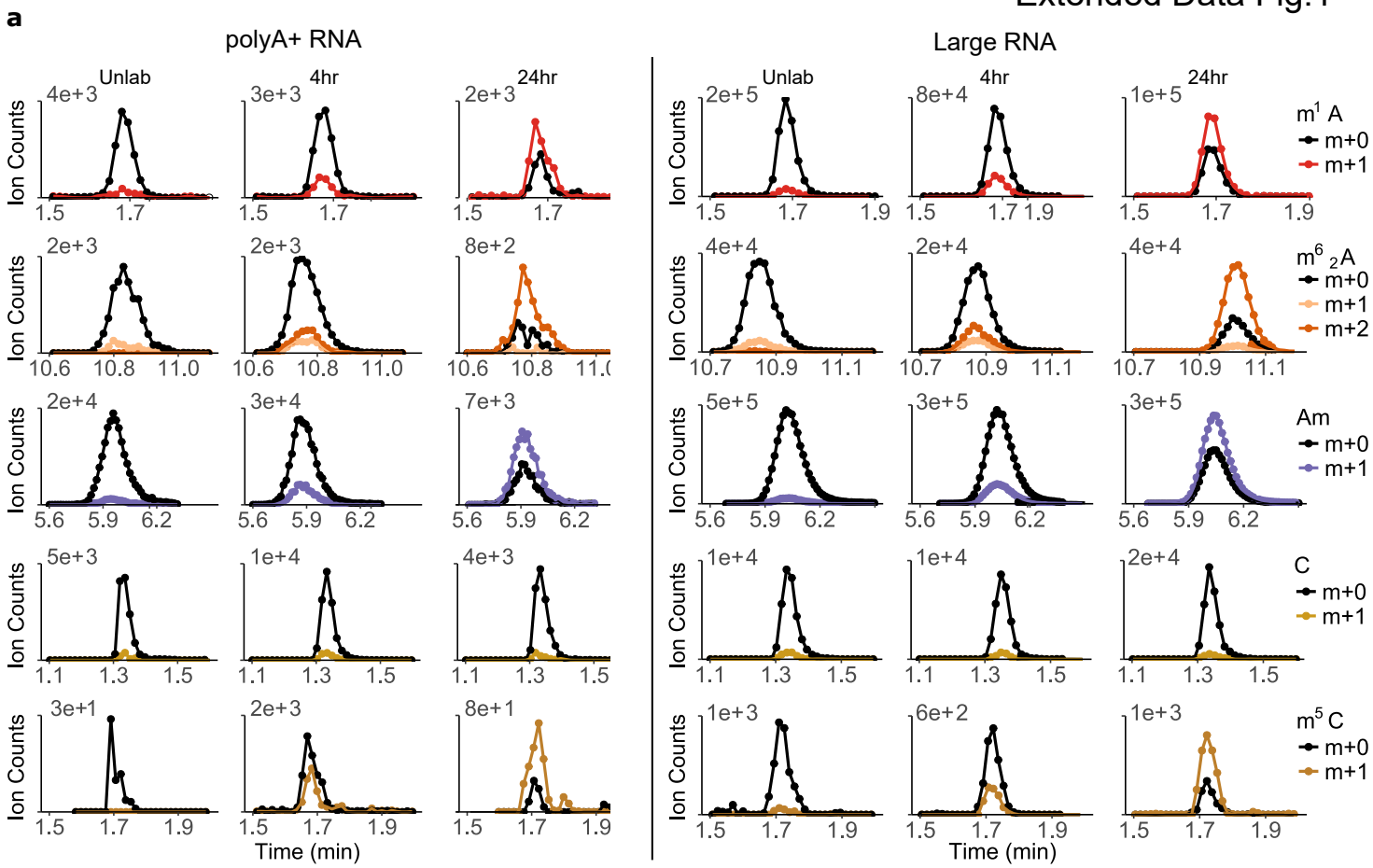


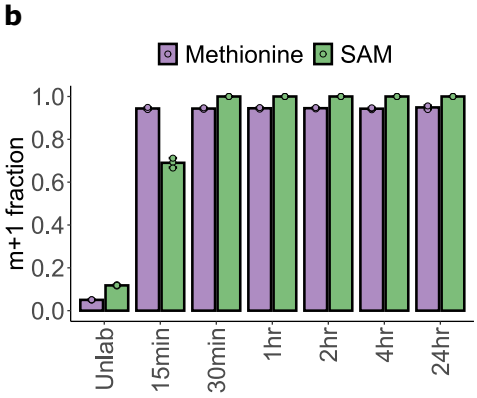


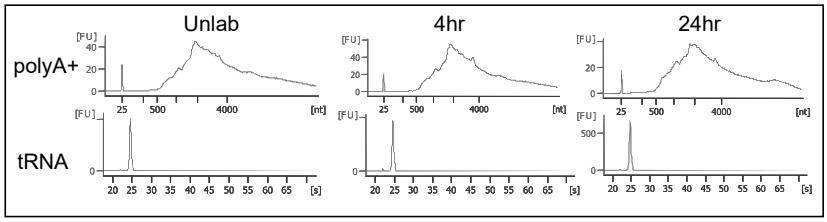


**Extended Data Fig 1. a,** The m+0 and m+1 isotopologues of $m^1A$, $m^6{}_2A$, Am, C and $m^5C$ (representative chromatograms) in polyA+ and large RNA following culture with either unlabelled methinine ('Unlab') or [13C-methyl]-methinine for 4 and 24 hours. **b,** $^{13}C$ labelling of intracellular methionine and SAM following culture with [$^{13}C$-methyl]-methinine for the indicated time periods. **c,** Representative bioanalyzer traces of polyA+ and tRNA samples. $m^1A$, 1-methyladenosine; $m^6{}_2A$, *N*6,*N*6-dimethyladenosine; Am, 2′-O-methyladenosine; C, cytidine; $m^5C$, 5-methylcytidine. Error bars represent 90% confidence intervals of three biological replicates in b.

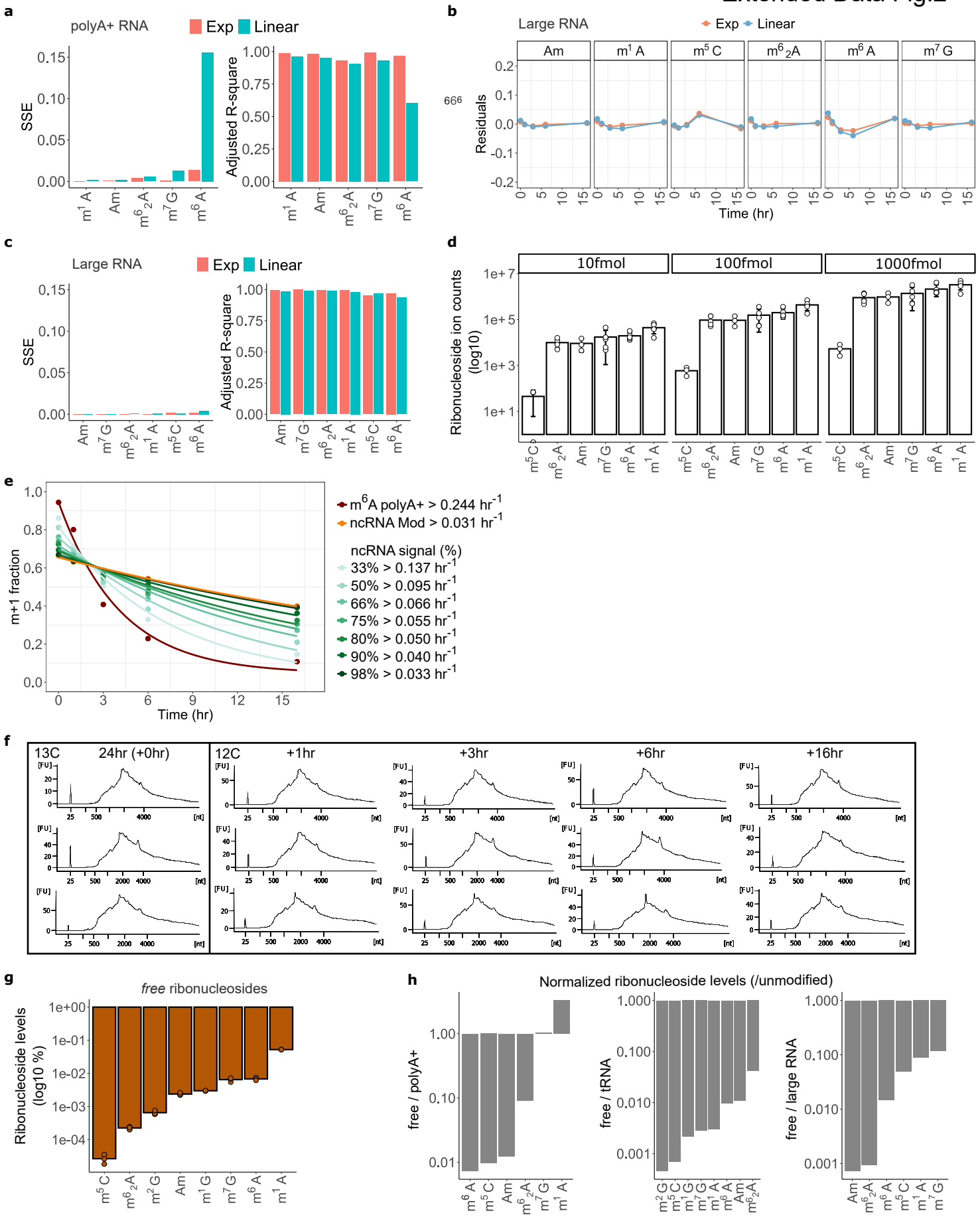


**Extended Data Fig 2. a-c,** Goodness-of-fit of a linear vs. exponential fit of isotopologue fractions determined in the chase experiment for polyA+ (a), and large RNA (b-c); SSE, sum of squared errors. **d,** Ion counts of equimolar analysis of pure ribonucleosides. **e,** Projected isotopologue fraction of a bona fide mRNA modification as measured in polyA+ RNA, with different degrees of ncRNA contamination. The effect on the isotopologue fraction over time was estimated from combinations of the m6A turnover in mRNA (0.244hr-1) with that of ncRNA (0.031hr-1, on average). **f,** Bioanalyzer traces of the polyA+ samples used in the chase experiments. **g,** Normalized ion counts of modified ribonucleosides relative to the ion counts sum of all ribonucleosides, in the free ribonucleoside pool. **h,** Ratio of normalised ion counts between free ribonucleosides and the different RNA classes. Error bars represent standard deviation of at least three biological replicates. In all cases, each replicate is the average of two technical replicas.

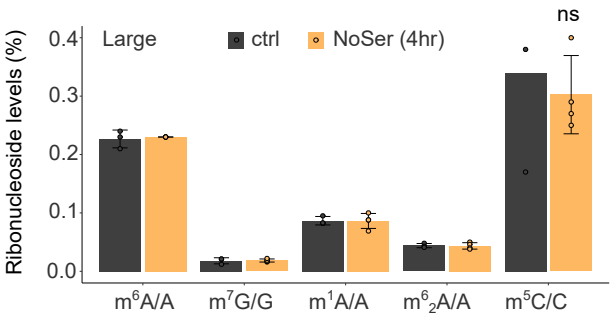


**Extended Data Fig 3.** Normalised abundance of modified ribonucleosides in large RNA, from 786O cells cultured with complete (ctrl) or serine- (NoSer) deprived DMEM medium for 4 hours. Error bars represent standard deviation of at least three biological replicates. In all cases, each replicate is the average of two technical replicas. ns, not significant, of a two-sided Student's t-Test comparing stress to ctrl conditions.

# Figures

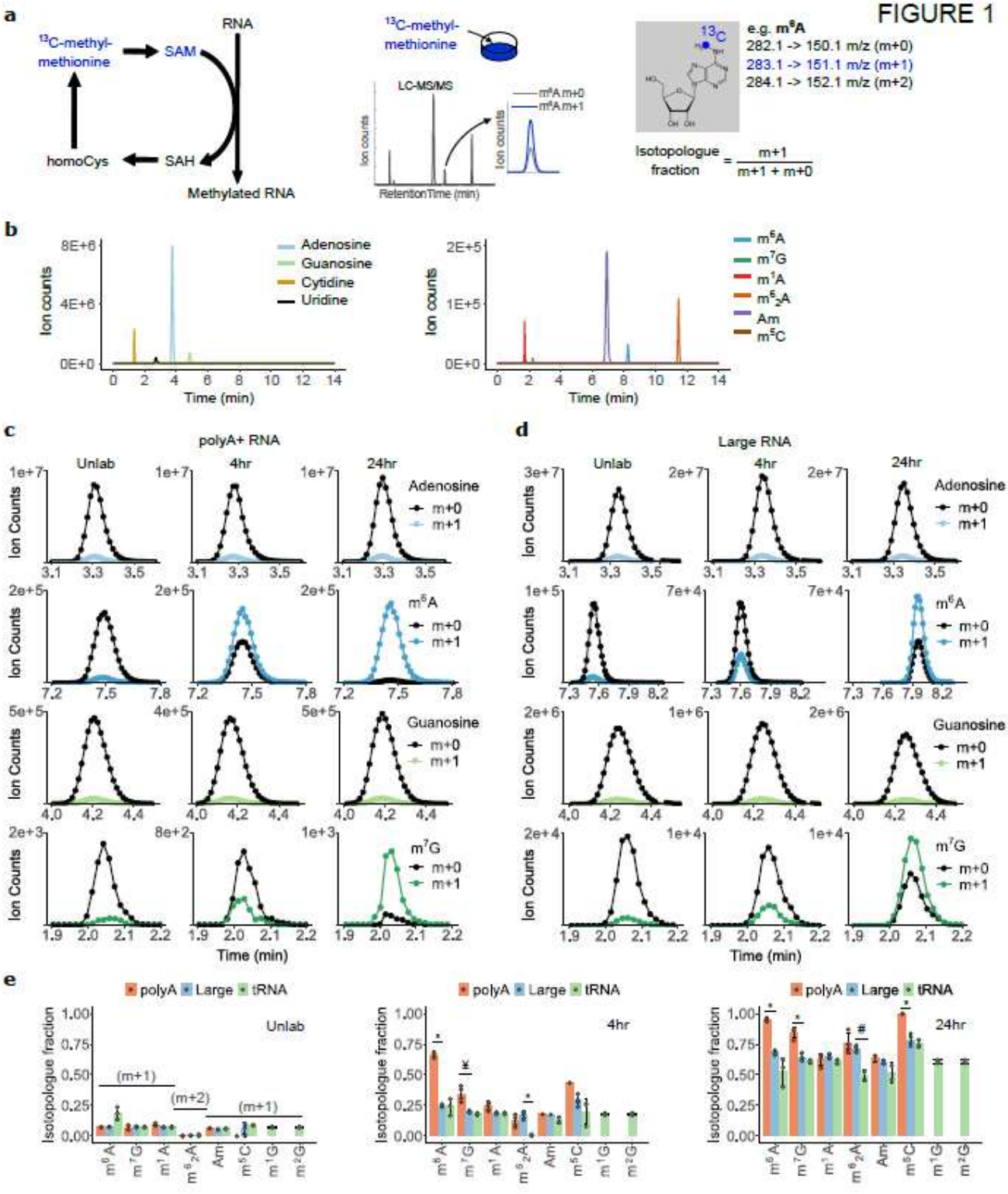


**Figure 1**

13C labelling of RNA modifications across RNA classes. a, The 13C-dynamods workflow shows the tracing of RNA methylation: cells are cultured with [13C-methyl]-methionine, the RNA is isolated, digested to ribonucleosides and subjected to LC-MS/MS analysis. The isotopologues detected for m6A are shown.

b, Representative chromatogram of unmodified and modified ribonucleosides from total RNA. c-d, The m+0 and m+1 isotopologues of modified and unmodified ribonucleosides (representative chromatograms) in polyA+ (c) and large RNA (d). e, Quantification of the isotopologue fractions of each ribonucleoside in polyA+, large and tRNA under unlabelled ('Unlab') conditions, after 4 and 24hours of culture with [13C-methyl]-methionine. m6A, N6-methyladenosine; m7G, 7-methylguanosine; m1A, 1-methyladenosine; m62A, N6,N6-dimethyladenosine; Am, 2'-O-methyladenosine; m5C, 5-methylcytidine; m1G, 1-methylguanosine; m2G, 2-methylguanosine. SAM, s-adenosylmethionine; SAH, s-adenosylhomocysteine; homoCys, homocysteine. Error bars represent standard deviation of three to four biological replicates, with the exception of two replicates for tRNA modifications. In all cases, each replicate is the average of two technical replicas. * denotes $P < 0.005$, ¥ denotes $P < 0.05$, # denotes $P = 0.059$, of a two-sided Student's t-Test comparing samples as indicated.

FIGURE 2

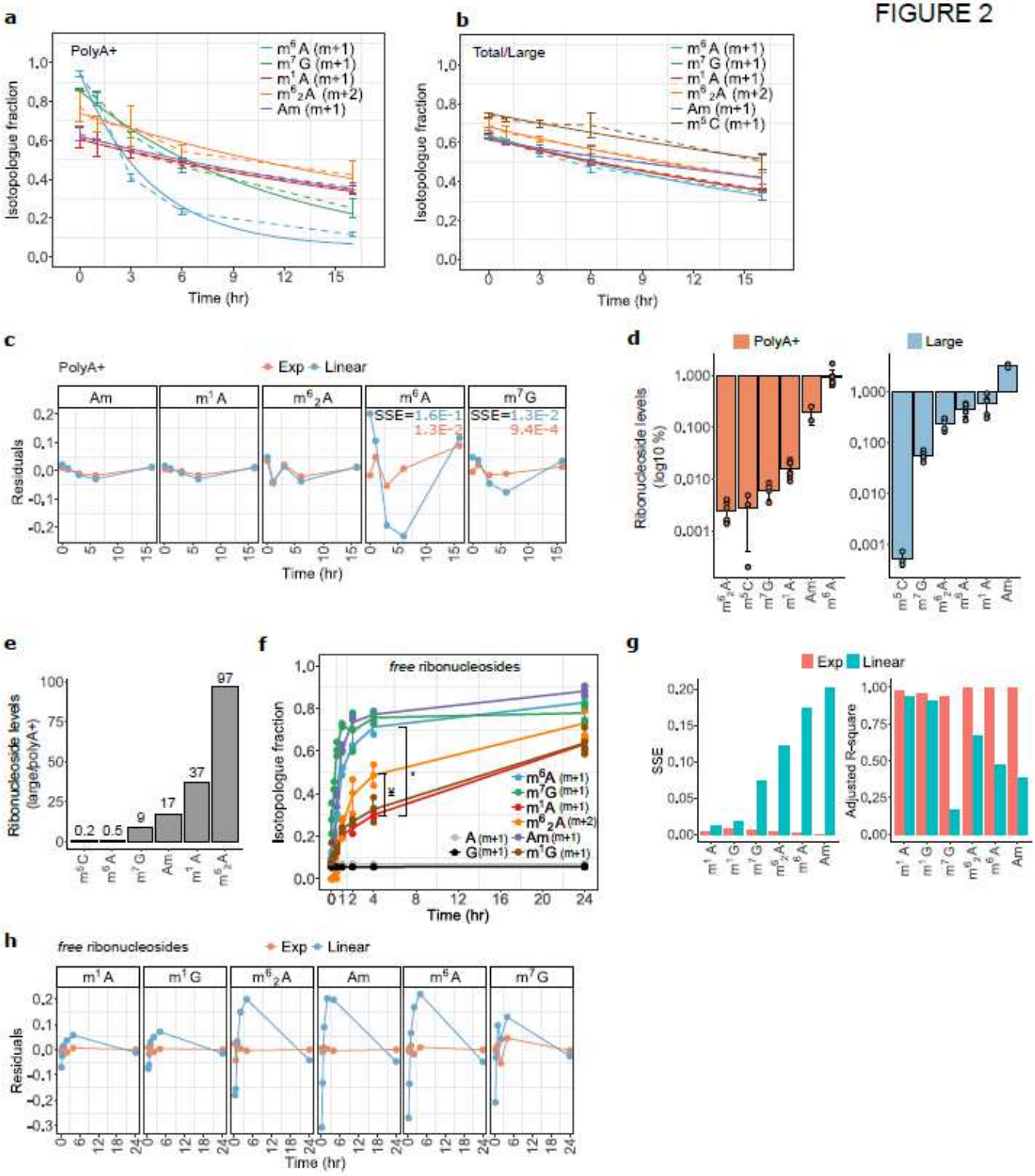


## Figure 2

Kinetic profiling of RNA modifications in polyA+, ncRNA and free ribonucleosides. a-b, Isotopologue fractions during the 'chase' of 13C-labelled modifications with naturally labelled methionine for 0, 1, 3, 6 and 16 hours, in polyA+ (a) and total/large RNA (b); dashed lines connect data points; solid lines, exponential (a) or linear (b) fit of isotopologue fractions. c, Residuals of a linear vs. exponential regression of isotopologue fractions in polyA+ RNA in the chase experiment. d, Normalized ion counts of

modified ribonucleosides relative to the ion counts sum of all ribonucleosides, shown for polyA+ and large RNA. (e) Ratio of normalised ion counts between polyA+ and large RNA, as determined in (d). f, Isotopologue fraction of free ribonucleosides analysed from metabolic extracts. g-h, Goodness-of-fit of a linear vs. exponential fit of the isotopologue fractions in free modified ribonucleosides. SSE, sum of squared errors. m6A, N6-methyladenosine; m7G, 7-methylguanosine; m1A, 1-methyladenosine; m62A, N6,N6-dimethyladenosine; Am, 2'-O-methyladenosine; m5C, 5-methylcytidine; m1G, 1-methylguanosine; A, adenosine; G, guanosine. Error bars represent 90%confidence intervals in (a-b), or standard deviation in (d, f) of at least three biological replicates with exception of Am (two replicates). In all cases, each replicate is the average of two technical replicas. * denotes P < 0.005, ¥ denotes P < 0.05, of a two-sided Student's t-Test comparing m6A and m62A to m1A, respectively.

FIGURE 3

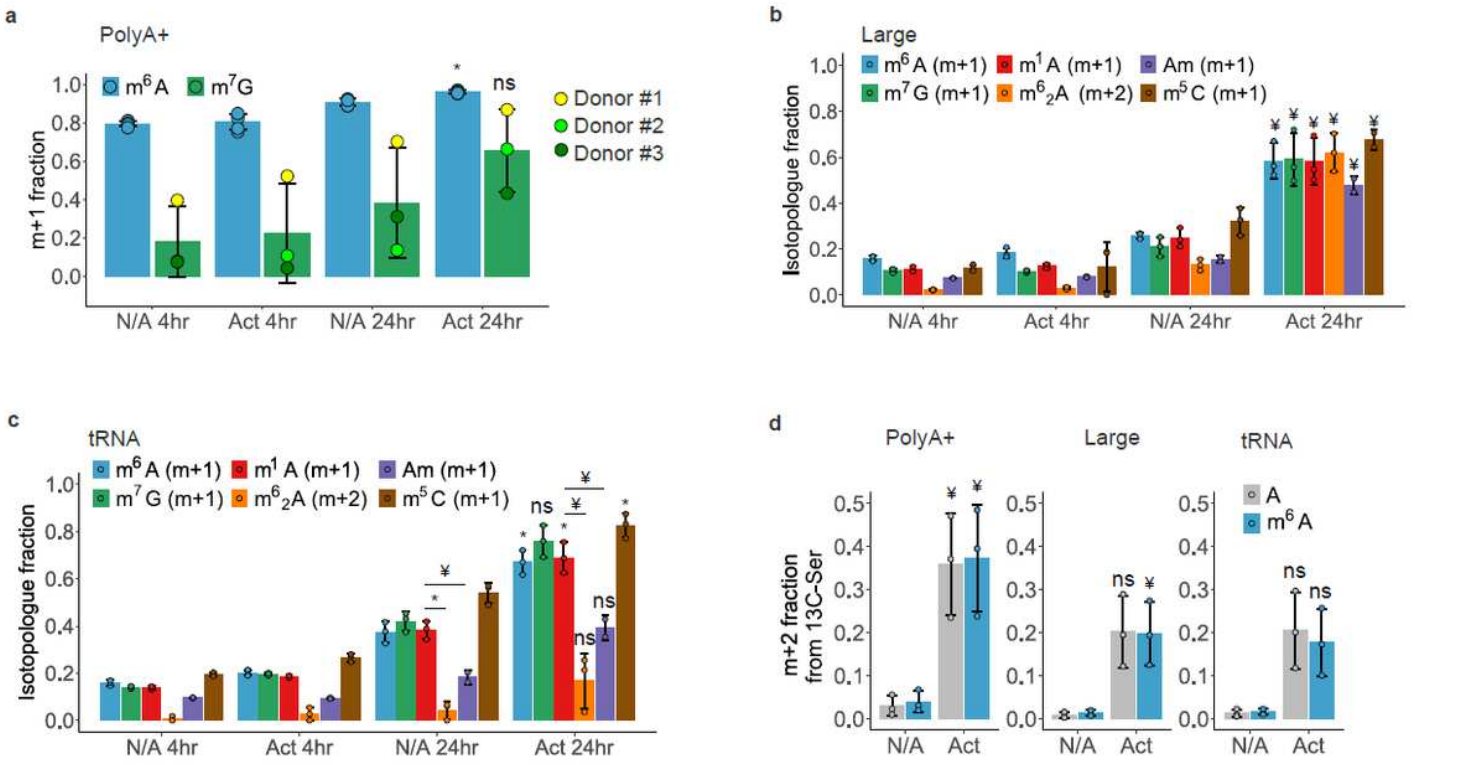


## Figure 3

RNA methylation dynamics during CD8+ T-cell activation. a-c, Isotopologue fractions of modified ribonucleosides in polyA+ (a), large (b) and tRNA (c) in CD8+ T-cells labelled with 13C-methyl-methionine for 4 and 24 hours and stimulated with CD3/CD28 antibodies for the same time period. d, Quantification of the m+2 fraction from [3-13C]serine. N/A, non-activated T-cells; Act, Activated T-cells for the times indicated. Error bars represent standard deviation of T-cell samples from three healthy donors. In all cases, each replicate is the average of two technical replicas. * denotes P < 0.005, ¥ denotes P < 0.05, ns denotes not significant, of a two-sided Student's t-Test comparing non-activated to activated T-cells at 24 hours or comparing modified ribonucleosides as indicated.

FIGURE 4

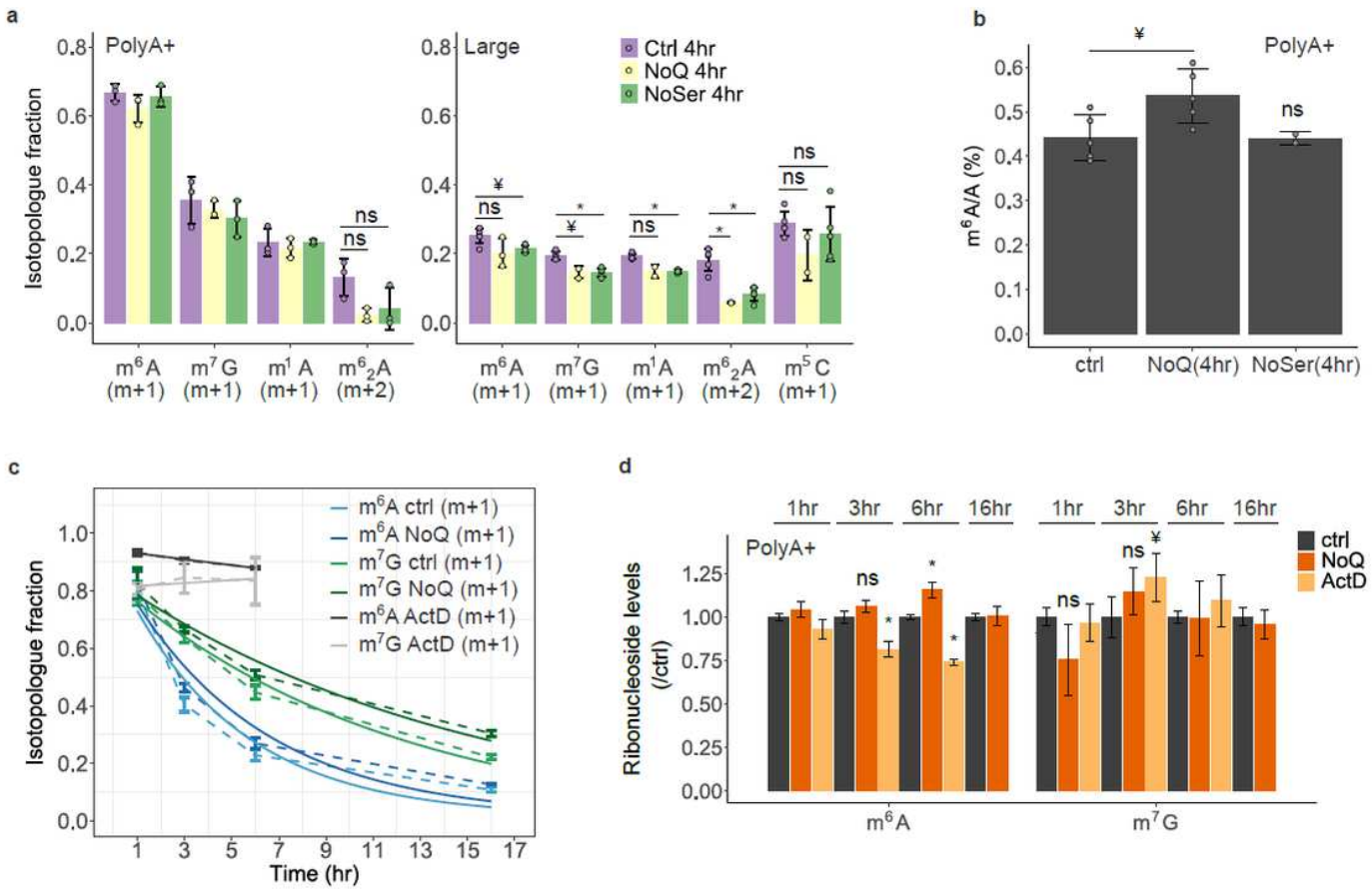


**Figure 4**

RNA methylation dynamics under metabolic stress. a, Isotopologue fractions of modified ribonucleosides in polyA+ and large RNA following [13C-methyl]-methionine labelling of 786O cells cultured with complete (ctrl), glutamine-(NoQ), or serine- (NoSer) deprived DMEM medium for 4 hours. b, Normalised levels of m6A relative to adenosine in polyA+ RNA from 786O cells cultured with ctrl, NoQ or NoSer DMEM medium for 4 hours. c, Isotopologue fractions of m6A and m7G in polyA+ RNA determined from the chase experiment in 786O cells cultured with ctrl, glutamine-deprived (NoQ) DMEM medium or treated with actinomycin D (ActD, 10μM); dashed lines connect data points; solid lines, exponential fit of isotopologue fractions. d, Levels of m6A and m7G in polyA+ RNA in the stress conditions as indicated, normalised relative to the ctrl condition in the chase experiment. Error bars represent standard deviation of three or more biological replicates, with exception of (c-d), m5C under NoQ (a) and m6A under NoSer (a) (two biological replicates). In all cases, each replicate is the average of two technical replicas. * denotes P < 0.005, ¥ denotes P < 0.05, ns denotes not significant, of a two-sided Student's t-Test comparing samples as indicated.

# Supplementary Files

This is a list of supplementary files associated with this preprint. Click to download.

- SupplementaryFile2SkylineDocsPeakDetectionIonChromatograms.rar